Janus faces of dipolar sources in directional near-field coupling with an oriented misalignment

Chenxu Bian [1,*] Yuhan Zhong,[1,*] Xuhuinan Chen,[1] Tony Low,[2,†] Hongsheng Chen,[1,3,‡] Baile Zhang,[4] and Xiao Lin [1,§]

[1]*State Key Laboratory of Extreme Photonics and Instrumentation, ZJU-Hangzhou Global Scientific and Technological Innovation Center,*
College of Information Science and Electronic Engineering, Zhejiang University, Hangzhou 310027, China
and International Joint Innovation Center, The Electromagnetics Academy at Zhejiang University,
Zhejiang University, Haining 314400, China
[2]*Department of Electrical and Computer Engineering, University of Minnesota, Minneapolis, Minnesota 55455, USA*
[3]*Key Lab of Advanced Micro/Nano Electronic Devices & Smart Systems of Zhejiang,*
Jinhua Institute of Zhejiang University, Zhejiang University, Jinhua 321099, China
and Shaoxing Institute of Zhejiang University, Zhejiang University, Shaoxing 312000, China
[4]*Division of Physics and Applied Physics, School of Physical and Mathematical Sciences,*
and Centre for Disruptive Photonic Technologies, Nanyang Technological University, Singapore 637371, Singapore

Directional near-field coupling can enable many applications, such as directional routing, on-chip information processing, and chiral quantum optics. This directional near-field coupling is generally face dependent, since the induced near-field radiation pattern is dependent on which face (e.g., the upper or lower face) of the dipolar source is facing toward the outcoupler. In other words, the dipolar sources in the directional near-field coupling intrinsically have two faces (e.g., Janus faces), whose corresponding near-field coupling strength and coupling directionality might be distinct. Here, we outline a general physical framework to control these Janus faces in the directional near-field coupling and find that they can have the feature of an oriented misalignment. To be specific, the upper and lower radiation patterns of excited surface waves can have the same shape but are misaligned with a twist angle. For example, the twist angle can be any acute angle if the source is composed of a Huygens dipole and an electric dipole, and it can be any obtuse angle if the source is constructed by a circular electric dipole and a magnetic dipole.

I. INTRODUCTION

Directional near-field coupling of dipolar sources [1–8] is of fundamental importance to tailor the flow of light at the subwavelength scale and has enabled many applications, such as chial quantum optics [9–13], on-chip information processing [14–17], and integrated light sources [18–21].

Since the near-field coupling strength and coupling directionality [22–29] are dependent on which face (e.g., the upper or lower face) of the dipolar source is facing toward the outcoupler (e.g., a waveguide), the resultant directional near-field coupling of dipolar sources is inherently face dependent. On one hand, some dipolar sources (e.g., Janus dipole) could have distinct coupling strengths for the upper and lower faces [30–33]. According to the recent studies reported in Ref. [30], if the Janus dipole is located in the middle of two parallel but spatially well-separated waveguides, the guided modes in the waveguide facing toward the upper face of the Janus dipole could be efficiently excited, while there is almost no excitation of guided modes in the other waveguide facing toward the lower face of the Janus dipole. Under this scenario, the upper face of the Janus dipole with the strong near-field coupling strength is then termed as the coupling face, while the lower face of the Janus dipole with very-weak near-field coupling stength is termed as the noncoupling face [34]. On the other hand, some dipolar sources (e.g., circular electric dipole and Huygens dipole) could have a face-dependent near-field coupling directionality. While the near-field directionalities induced by the upper and lower faces are opposite for the circular electric dipole [30,31,35], they are the same for the Huygens dipole [30,31,34]. In short, the dipolar sources inherently have Janus faces in the near-field coupling. Since the existence of Janus coupling indicates new possibilities to flexibly engineer the coupling strength and coupling directionality in space, the manipulation of these Janus faces would serve to enrich the physics of light-matter interactions and form various exotic near-field coupling phenomena. However, a general physical framework for near-field directional Janus coupling is lacking.

II. CACULATIONS FOR TWIST ANGLE

Here we reveal a feasible framework to flexibly tailor the Janus faces of dipolar sources in the directional near-field coupling and find that these Janus faces could have the feature of an oriented misalignment. That is, the radiation patterns of surface waves induced by the upper and lower coupling faces of a complex dipolar source could have the same shape but are misaligned with a twist angle. This twist angle then manifests the unique spatial correspondence

---

*These authors contributed equally to this work.

†tlow@umn.edu

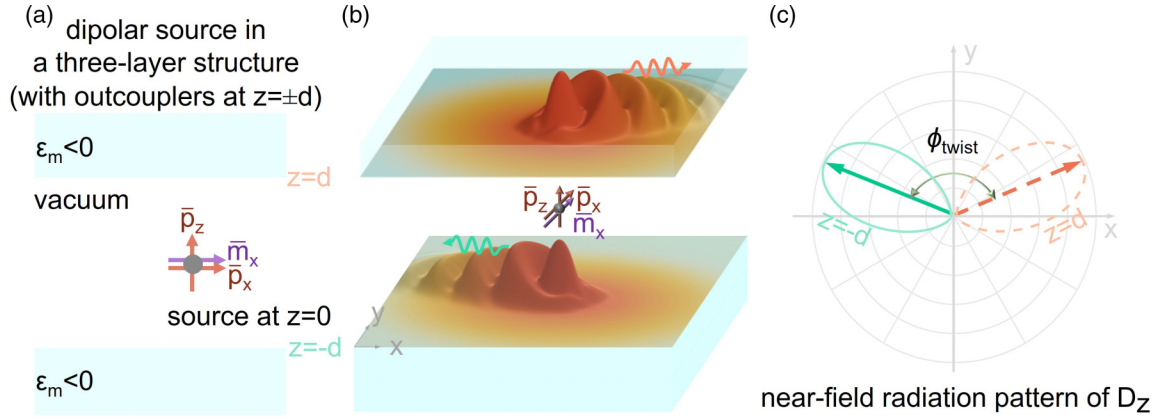‡hansomchen@zju.edu.cn

§xiaolinzju@zju.edu.cn

FIG. 1. Conceptual illustration of Janus faces of dipolar sources in the directional near-field coupling with an oriented misalignment. (a) Structural schematic. To manifest the Janus faces in the near-field coupling, one outcoupler is deposited in the upper side of the dipolar source, while the other one is in the lower side. Each outcoupler supports the propagation of TM surface waves and can be constructed, for example, by the optical interface between vacuum and a negative-permittivity material (e.g., metal with a relative permittivity of ε_m). (b), (c) Conceptual illustration of Janus faces of dipolar sources. The near-field radiation patterns of the excited TM surface waves on the upper and lower interfaces are calculated by using $|D_{z,\mathrm{sw},z=d}^{\mathrm{upper}}(\phi)|$ and $|D_{z,\mathrm{sw},z=-d}^{\mathrm{lower}}(\phi)|$, respectively. These radiation patterns have the same shape but have the feature of an oriented misalignment, and this twist angle also corresponds to the angle between the angular direction having $\max[|D_{z,\mathrm{sw},z=d}^{\mathrm{upper}}(\phi)|]$ (orange arrow) and that having $\max[|D_{z,\mathrm{sw},z=-d}^{\mathrm{lower}}(\phi)|]$ (green arrow).

between the face-dependent near-field directionalities induced by the same dipolar source. Moreover, we find that Janus faces with an arbitrary twist angle in the directional near-field coupling are achievable via the judicious design of the source's dipolar constituents.

Figure 1 conceptually illustrates the Janus faces of dipolar sources in the directional near-field coupling with an oriented misalignment. To manifest the face-dependent near-field coupling, the optical interface between vacuum and a negative-permittivity material (e.g., metal) is chosen as the outcoupler, which supports the propagation of transverse-magnetic (TM) surface waves in the x-y plane. For illustration, the dipolar source is composed of an electric dipole moment $\bar{p} = \hat{x}p_x + \hat{z}p_z$ and a magnetic dipole moment $\bar{m} = \hat{x}m_x$, and it is located inside the vacuum region with a vertical distance of $d = 0.5\lambda_0$ to the designed interface, where λ_0 is the working wavelength in vacuum. For dipolar sources simultaneously possessing the electric and magnetic dipole moments, they can be achieved in practice by exploiting the antenna design at the microwave regime [36–39], plasmonic scatterer nanostructures with electric and magnetic response [40–42], or high-index dielectric nanoparticles in the Rayleigh regime [43–47].

The field distribution of excited surface waves can then be analytically derived, readily by following the classic electromagnetic wave theory and by enforcing the boundary conditions [48–54]. If the optical interface is at $z = d$ and located at the upper side of the source, the field distribution of electric displacement D_z of the excited TM surface waves at this upper interface can be obtained as $D_{z,\mathrm{sw},z=d}^{\mathrm{upper}}(\phi) = D_0[\frac{k_0}{k_{z,\mathrm{sw}}}\frac{m_x}{c}\sin\phi - p_x\cos\phi + p_z\frac{k_{\rho,\mathrm{sw}}}{k_{z,\mathrm{sw}}}]$, where $\bar{k}_{\mathrm{sw}} = \hat{\rho}k_{\rho,\mathrm{sw}} + \hat{z}k_{z,\mathrm{sw}}$ is the wave vector of the excited surface wave in the region of vacuum, $k_{z,\mathrm{sw}} = \sqrt{k_0^2 - k_{\rho,\mathrm{sw}}^2}$, $\phi \in [0°, 360°]$ is the angle between $\hat{\rho}k_{\rho,\mathrm{sw}}$ and the unit vector $\hat{x}$, D_0 is a ϕ-independent factor (see Appendix C), $k_0 = \omega/c$,

ω is the angular frequency, and c is the speed of light in vacuum. Below we consider the case with $\sqrt{1 + \left(\frac{k_0}{k_{z,\mathrm{sw}}}\frac{m_x/c}{p_x}\right)^2} \neq 0$; see the discussion about the case with $\sqrt{1 + \left(\frac{k_0}{k_{z,\mathrm{sw}}}\frac{m_x/c}{p_x}\right)^2} = 0$ in Appendix F. Accordingly, this induced field at the upper interface can be reexpressed as

$$D_{z,\mathrm{sw},z=d}^{\mathrm{upper}}(\phi) = D_0 p_x \sqrt{1 + \left(\frac{k_0}{k_{z,\mathrm{sw}}}\frac{m_x/c}{p_x}\right)^2}$$
$$\times \left[\sin(\phi + \phi_0) + \frac{\frac{k_{\rho,\mathrm{sw}}}{k_{z,\mathrm{sw}}}\frac{p_z}{p_x}}{\sqrt{1 + \left(\frac{k_0}{k_{z,\mathrm{sw}}}\frac{m_x/c}{p_x}\right)^2}}\right], \quad (1)$$

where ϕ_0 is a constant angle with

$$\sin\phi_0 = \frac{-1}{\sqrt{1 + \left(\frac{k_0}{k_{z,\mathrm{sw}}}\frac{m_x/c}{p_x}\right)^2}}$$

and

$$\cos\phi_0 = \frac{\frac{k_0}{k_{z,\mathrm{sw}}}\frac{m_x/c}{p_x}}{\sqrt{1 + \left(\frac{k_0}{k_{z,\mathrm{sw}}}\frac{m_x/c}{p_x}\right)^2}}.$$

Since $k_{\rho,\mathrm{sw}}$ would be purely real and $k_{z,\mathrm{sw}}$ would be purely imaginary for the TM surface wave under the lossless condition, the value of ϕ_0 in Eq. (1) would be a real number if $\frac{m_x/c}{p_x}$ is purely imaginary. Then we can express $\phi_0 = 90° - \arctan(-\frac{k_0}{k_{z,\mathrm{sw}}}\frac{m_x/c}{p_x}) + m \times 180°$, where $m = 0$ or 1 to ensure $\phi_0 \in [0°, 360°]$. Furthermore, the field of $D_{z,\mathrm{sw},z=d}^{\mathrm{upper}}(\phi)$ could be highly asymmetric with respect to ϕ, namely,

$$\left|\frac{D_{z,\mathrm{sw},z=d}^{\mathrm{upper}}(\phi = 90° - \phi_0)}{D_{z,\mathrm{sw},z=d}^{\mathrm{upper}}(\phi = 270° - \phi_0)}\right| \gg 1$$

or

$$\left| \frac{D_{z,\text{sw},z=d}^{\text{upper}}(\phi = 90° - \phi_0)}{D_{z,\text{sw},z=d}^{\text{upper}}(\phi = 270° - \phi_0)} \right| \ll 1,$$

if $\frac{p_z}{p_x}$ is purely imaginary. In other words, we can realize the near-field directionality at the upper interface under the condition of both $\frac{m_x/c}{p_x}$ and $\frac{p_z}{p_x}$ being purely imaginary. Note that if $p_x = 0$, these conditions are equivalent to $\frac{m_x/c}{p_z}$ being purely real. Under the occurrence of this near-field directionality, the angular direction with the maximum radiation has $|D_{z,\text{sw},z=d}^{\text{upper}}(\phi = \phi_{\max}^{\text{upper}})| = \max(|D_{z,\text{sw},z=d}^{\text{upper}}(\phi)|)$, where $\phi_{\max}^{\text{upper}} = \mod(90° - \phi_0, 360°)$ if

$$\frac{\frac{k_{\rho,\text{sw}}}{k_{z,\text{sw}}}\frac{p_z}{p_x}}{\sqrt{1 + \left(\frac{k_0}{k_{z,\text{sw}}}\frac{m_x/c}{p_x}\right)^2}} > 0$$

in Eq. (1) and $\phi_{\max}^{\text{upper}} = \mod(270° - \phi_0, 360°)$ if

$$\frac{\frac{k_{\rho,\text{sw}}}{k_{z,\text{sw}}}\frac{p_z}{p_x}}{\sqrt{1 + \left(\frac{k_0}{k_{z,\text{sw}}}\frac{m_x/c}{p_x}\right)^2}} < 0.$$

If the optical interface is at $z = -d$ and located at the lower side of the source, the induced field distribution of excited TM surface waves at this lower interface can be

obtained as

$$D_{z,\text{sw},z=-d}^{\text{lower}}(\phi) = D_0 p_x \sqrt{1 + \left(\frac{k_0}{k_{z,\text{sw}}}\frac{m_x/c}{p_x}\right)^2}$$

$$\times \left[\sin(\phi - \phi_0) + \frac{\frac{k_{\rho,\text{sw}}}{k_{z,\text{sw}}}\frac{p_z}{p_x}}{\sqrt{1 + \left(\frac{k_0}{k_{z,\text{sw}}}\frac{m_x/c}{p_x}\right)^2}} \right]. \tag{2}$$

Similarly, when both $\frac{m_x/c}{p_x}$ and $\frac{p_z}{p_x}$ are purely imaginary if $p_x \neq 0$ or when $\frac{m_x/c}{p_z}$ is purely real if $p_x = 0$, the near-field directionality can also emerge at this lower optical interface. Accordingly, when we denote $|D_{z,\text{sw},z=-d}^{\text{lower}}(\phi = \phi_{\max}^{\text{lower}})| = \max(|D_{z,\text{sw},z=-d}^{\text{lower}}(\phi)|)$ for this near-field directionality, we have $\phi_{\max}^{\text{lower}} = \mod(90° + \phi_0, 360°)$ if

$$\frac{\frac{k_{\rho,\text{sw}}}{k_{z,\text{sw}}}\frac{p_z}{p_x}}{\sqrt{1 + \left(\frac{k_0}{k_{z,\text{sw}}}\frac{m_x/c}{p_x}\right)^2}} > 0$$

in Eq. (2) and $\phi_{\max}^{\text{lower}} = \mod(270° + \phi_0, 360°)$ if

$$\frac{\frac{k_{\rho,\text{sw}}}{k_{z,\text{sw}}}\frac{p_z}{p_x}}{\sqrt{1 + \left(\frac{k_0}{k_{z,\text{sw}}}\frac{m_x/c}{p_x}\right)^2}} < 0.$$

Upon close inspection of Eqs. (1) and (2), mathematically, we have

$$\left| D_{z,\text{sw},z=d}^{\text{upper}}(\phi) \right| = \left| D_{z,\text{sw},z=-d}^{\text{lower}}(\phi - \phi_{\text{twist}}) \right| \quad \text{or} \quad \left| D_{z,\text{sw},z=d}^{\text{upper}}(\phi) \right| = \left| D_{z,\text{sw},z=-d}^{\text{lower}}(\phi + \phi_{\text{twist}}) \right|, \tag{3}$$

where

$$\phi_{\text{twist}} = \begin{cases} \left| \phi_{\max}^{\text{lower}} - \phi_{\max}^{\text{upper}} \right|, & \text{if } \left| \phi_{\max}^{\text{lower}} - \phi_{\max}^{\text{upper}} \right| \in [0°, 180°] \\ 360° - \left| \phi_{\max}^{\text{lower}} - \phi_{\max}^{\text{upper}} \right|, & \text{if } \left| \phi_{\max}^{\text{lower}} - \phi_{\max}^{\text{upper}} \right| \in [180°, 360°] \end{cases}. \tag{4}$$

Equation (3) indicates that the upper and lower radiation patterns of excited surface waves have the same shape and near-field directionality but have an oriented misalignment with a twist angle. According to the definition of twist angle in Eq. (4), we always have $\phi_{\text{twist}} \in [0°, 180°]$.

With the knowledge of $\phi_{\max}^{\text{upper}}$ and $\phi_{\max}^{\text{lower}}$, Eq. (4) can be rewritten as

$$\phi_{\text{twist}} = \begin{cases} 180° - 2\arctan\left(-\frac{k_0}{k_{z,\text{sw}}}\frac{m_x}{c}\frac{1}{p_x}\right), & \text{if } \arctan\left(-\frac{k_0}{k_{z,\text{sw}}}\frac{m_x/c}{p_x}\right) \in [0°, 90°] \\ 180° + 2\arctan\left(-\frac{k_0}{k_{z,\text{sw}}}\frac{m_x/c}{p_x}\right), & \text{if } \arctan\left(-\frac{k_0}{k_{z,\text{sw}}}\frac{m_x/c}{p_x}\right) \in [-90°, 0°] \end{cases}. \tag{5}$$

Equation (5) indicates that the twist angle between the induced near-field directionalities in the lower and upper interfaces is merely determined by the factor $-\frac{k_0}{k_{z,\text{sw}}}\frac{m_x/c}{p_x}$, irrelevant to p_z. This is despite the fact that the near-field directionality at the lower or upper interface, as governed by Eqs. (1) and (2), originates from the interference of all evanescent waves induced by p_x, m_x, and p_z. The underlying reason is that the distribution of evanescent waves induced by p_z has the rotational symmetry in the x-y plane and is thus ϕ independent, while that induced by p_x and m_x has the odd symmetry in the x-y plane and is thus ϕ dependent. This way, under the existence of p_z, the Janus faces of dipolar sources with an arbitrary twist angle in the directional near-field coupling are achievable by the judicious design of dipolar constituents

p_x and m_x. We point out that the Janus faces of dipolar sources with an arbitrary twist angle in the directional near-field coupling revealed in this work have not been thoroughly investigated, despite the recent investigation on the flexible manipulation of both the amplitude and phase of guided modes excited by a dipolar source [30,54,55] and recently the extensive studies of twistronics [56–62] and twisted optics [63–72].

Holding upon these general arguments, we show the possibility to realize Janus faces of dipolar sources in the directional near-field coupling with a twist angle of $\phi_{\text{twist}} = 0°$ in Fig. 2(a), $\phi_{\text{twist}} = 90°$ in Fig. 2(b), and $\phi_{\text{twist}} = 180°$ in Fig. 2(c). To facilitate the conceptual illustration, below the negative-permittivity material is set to have a relative
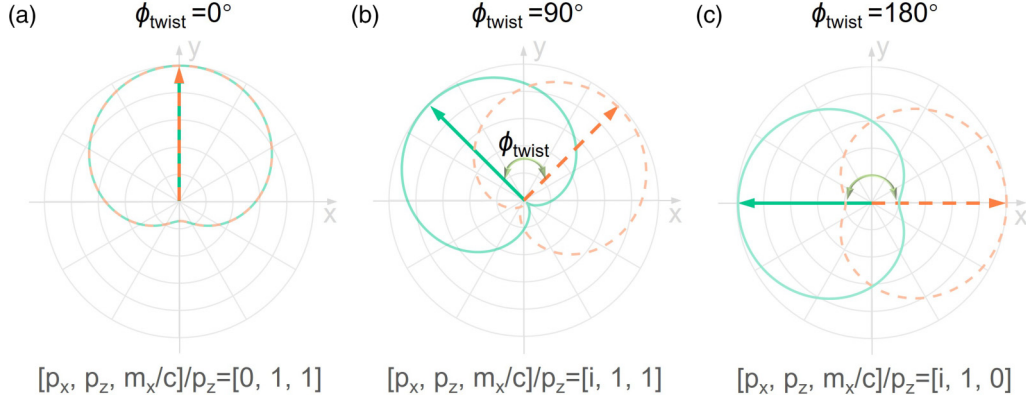
FIG. 2. Janus faces of dipolar sources in the directional near-field coupling with a twist angle of $0°$, $90°$, or $180°$ by plotting the near-field radiation patterns. The structural setup is the same as Fig. 1 with the use of $\varepsilon_m = -2$. The dipolar source is composed of an electric dipole moment $\bar{p} = \hat{x}p_x + \hat{z}p_z$ and a magnetic dipole moment $\bar{m} = \hat{x}m_x$. (a) $\phi_{\text{twist}} = 0°$, if a Huygens dipole is used, namely, $[p_x, p_z, m_x/c]/p_z = [0, 1, 1]$. (b) $\phi_{\text{twist}} = 90°$, if $[p_x, p_z, m_x/c]/p_z = [i, 1, 1]$. (c) $\phi_{\text{twist}} = 180°$, if a circular electric dipole is used, namely, $[p_x, p_z, m_x/c]/p_z = [i, 1, 0]$. Here and below, $p_z = 1$ C m is used.

permittivity of -2. Then, we have $-\frac{k_0}{k_{z,\text{sw}}} = i$ in Eq. (5), and Eq. (5) can be reduced to

$$\phi_{\text{twist}} = \begin{cases} 180° - 2\arctan\frac{m_x/c}{-ip_x}, & \text{if } \frac{m_x/c}{-ip_x} \geqslant 0 \\ 180° + 2\arctan\frac{m_x/c}{-ip_x}, & \text{if } \frac{m_x/c}{-ip_x} < 0 \end{cases}. \quad (6)$$

When $\phi_{\text{twist}} = 0°$ in Fig. 2(a), this requires $\frac{m_x/c}{-ip_x} \rightarrow +\infty$ in Eq. (6). Accordingly, the dipolar source has $[p_x, p_z, m_x/c]/p_z = [0, 1, 1]$. This kind of dipolar source is exactly the Huygens dipole, whose electric and magnetic dipole moments are in phase and orthogonal to each other, along with the ratio between their magnitudes fulfilling Kerker's condition of $\frac{|\bar{m}|}{|\bar{p}|} = c$ [73–76]. When $\phi_{\text{twist}} = 180°$ in Fig. 2(c), $\frac{m_x/c}{-ip_x} = 0$ is needed, and the dipolar source starts to have $[p_x, p_z, m_x/c]/p_z = [i, 1, 0]$. This kind of dipolar source is exactly the circular electric dipole, whose two electric dipole moments are $90°$ out of phase and orthogonal to each other and they have the same magnitude. Similarly, when $\phi_{\text{twist}} = 90°$ in Fig. 2(b), $\frac{m_x/c}{-ip_x} = 1$ should be satisfied. That is, the dipolar source has $[p_x, p_z, m_x/c]/p_z = [i, 1, 1]$. Since $[p_x, p_z, m_x/c]/p_z = [0, 1, 1]_{\text{Huygens dipole}} + [i, 0, 0]_{\text{electric dipole}} = [i, 1, 0]_{\text{circular electric dipole}} + [0, 0, 1]_{\text{magnetic dipole}}$, this dipolar source in Fig. 2(b) can be equivalently treated as the combination of a Huygens dipole and an electric dipole or the combination of a circular electric dipole and a magnetic dipole.

With the knowledge of Fig. 2, we now proceed to discuss the possibility to realize Janus faces of dipolar sources with an arbitrary twist angle in the directional near-field coupling. To fulfill the condition of $\frac{p_x}{p_z}$ being purely imaginary and $\frac{m_x/c}{p_z}$ being purely real, we can let $[p_x, p_z, m_x/c]/p_z = [a_e i, 1, b_m]$, where a_e and b_m are both real numbers. For conceptual illustration, below we consider the case with $a_e > 0$ and $b_m > 0$. Then, the twist angle in Eq. (6) can be simplified to

$$\phi_{\text{twist}} = 180° - 2\arctan\frac{b_m}{a_e}. \quad (7)$$

Equation (7) indicates that the twist angle would vary from $0°$ to $90°$, if the factor $\frac{b_m}{a_e}$ changes from 1 to $+\infty$; see the

blue dash-dotted curve in Fig. 3. For example, if $a_e = 0.42$ and $b_m = 1$, we have $\phi_{\text{twist}} = 45°$, which is numerically verified by the corresponding field distribution of excited TM surface waves in the upper and lower interfaces in Fig. 4(a). Particularly, if $b_m = 1$, the source's dipolar constituents can be reexpressed as

$$[p_x, p_z, m_x/c]/p_z$$
$$= [0, 1, 1]_{\text{Huygens dipole}} + a_e[i, 0, 0]_{\text{electric dipole}}. \quad (8)$$

Equation (8) indicates that the combination of a Huygens dipole and an electric dipole could be exploited to realize any twist angle within the range of $0°-90°$.

Similarly, the twist angle would vary from $90°$ to $180°$, if the factor $\frac{b_m}{a_e}$ changes from 0 to 1, as shown by the orange dashed curve in Fig. 3. As a typical example, we have
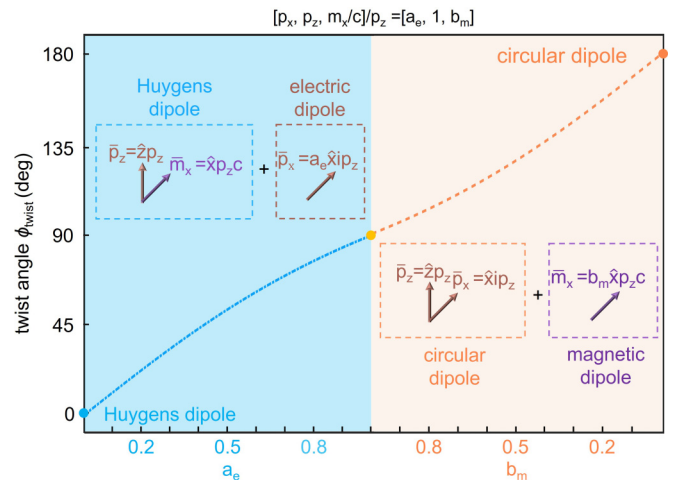

FIG. 3. Realization of Janus faces of dipolar sources in the directional near-field coupling with an arbitrary twist angle. If the dipolar source is composed of a Huygens dipole and an electric dipole, the twist angle can vary from $0°$ to $90°$; see the blue dash-dotted curve. If the dipolar source is constructed by a circular electric dipole and a magnetic dipole, the twist angle can vary from $90°$ to $180°$; see the orange dashed curve.
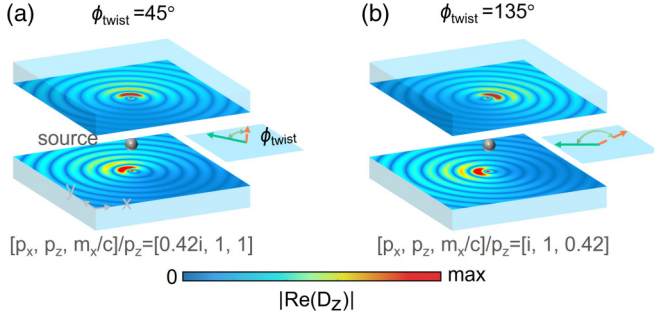
FIG. 4. Demonstration of Janus faces of dipolar sources in the directional near-field coupling with a twist angle of $45°$ or $135°$ by plotting the field distribution of excited surface waves. The structural setup is the same as Fig. 1 with the use of $\varepsilon_m = -2$. (a) $\phi_{\text{twist}} = 45°$, if the dipolar source is constructed by $[p_x, p_z, m_x/c]/p_z = [0.42i, 1, 1]$. (b) $\phi_{\text{twist}} = 135°$, if the dipolar source is composed of $[p_x, p_z, m_x/c]/p_z = [i, 1, 0.42]$.

$\phi_{\text{twist}} = 135°$ if $a_e = 1$ and $b_m = 0.42$; see the corresponding field distribution of excited surface waves in the lower and upper interfaces in Fig. 4(b). Moreover, if $a_e = 1$ is used, the source's dipolar constituents can also be reexpressed as

$$[p_x, p_z, m_x/c]/p_z = [i, 1, 0]_{\text{circular electric dipole}}$$
$$+ b_m[0, 0, 1]_{\text{magnetic dipole}}. \quad (9)$$

Equation (9) shows that the combined usage of a circular electric dipole and a magnetic dipole can help to achieve Janus faces of dipolar sources with a twist angle of $\phi_{\text{twist}} \in [90°, 180°]$ in the directional near-field coupling.

III. CONCLUSION

In conclusion, we have revealed the emergence of Janus faces of dipolar sources with an oriented misalignment, by engineering the face-dependent near-field directionality. We have found that the upper and lower radiation patterns of excited surface waves could possess the same shape but with a twist angle, whose value can be arbitrary and achievable via judiciously designing the dipolar constituents. We have found that Janus faces of dipolar sources in the directional near-field coupling with a twist angle in the range of $0°-90°$ can be achieved by exploiting the combination of a Huygens dipole and an electric dipole, and those in the range of $90°-180°$ can be realized by using the combination of a circular electric dipole and a magnetic dipole. Due to the intrinsic Janus faces of dipolar sources in the directional near-field coupling, our finding may offer an extra degree of freedom for the design of advanced on-chip applications, such as face-dependent directional routing and face-dependent on-chip information processing. Looking forward, while this work is focused on the case that has the same upper and lower near-field radiation patterns but with an arbitrary twist angle, more intriguing cases (e.g., having different upper and lower radiation patterns but with an arbitrary twist angle) could in principle be achieved by exploiting other dipolar or high-order sources (e.g., quadrupoles [77]), which await further explorations.

The data that support the findings of this study are available from the corresponding author upon reasonable request.

APPENDIX A: FIELD DISTRIBUTION OF A DIPOLAR SOURCE IN HOMOGENEOUS MATTER

In this section, we give a detailed derivation of the field distribution, if the dipolar source is inside a homogeneous medium. We begin with Maxwell's equations, namely,

$$\nabla \times \bar{E}(\bar{r}) = i\omega\mu\bar{H}(\bar{r}), \quad (A1)$$

$$\nabla \times \bar{H}(\bar{r}) = -i\omega\varepsilon\bar{E}(\bar{r}) + \bar{J}(\bar{r}), \quad (A2)$$

where $\mu = \mu_0\mu_r$; $\varepsilon = \varepsilon_0\varepsilon_r$; ε_0 and μ_0 are the permittivity and permeability of vacuum, respectively; ε_r and μ_r are the relative permittivity and permeability for the homogeneous medium where dipolar source locates, respectively.

From Eqs; (A1) and (A2), we can obtain the following equation for $\bar{E}(\bar{r})$:

$$\nabla \times \nabla \times \bar{E}(\bar{r}) - k^2\bar{E}(\bar{r}) = i\omega\mu\bar{J}(\bar{r}). \quad (A3)$$

To solve Eq. (A3), we can express the electric field $\bar{E}(\bar{r})$ by the dyadic Green's functions $\bar{\bar{G}}(\bar{r}, \bar{r}')$:

$$\bar{E}(\bar{r}) = i\omega\mu \iiint d\bar{r}' \bar{\bar{G}}(\bar{r}, \bar{r}')\bar{J}(\bar{r}'). \quad (A4)$$

Similarly, for the source in Eq. (A4), $\bar{J}(\bar{r}')$ can be expressed as

$$\bar{J}(\bar{r}) = \iiint d\bar{r}' \delta(\bar{r} - \bar{r}')\bar{\bar{I}}\bar{J}(\bar{r}'). \quad (A5)$$

By substituting Eqs. (A4) and (A5) into Eq. (A3), one obtains

$$\nabla \times \nabla \times \bar{\bar{G}}(\bar{r}, \bar{r}') - k^2\bar{\bar{G}}(\bar{r}, \bar{r}') = \bar{\bar{I}}\delta(\bar{r} - \bar{r}'). \quad (A6)$$

From Eq. (A6), we can further express $\bar{\bar{G}}(\bar{r}, \bar{r}')$ by the scalar Green's function as

$$\bar{\bar{G}}(\bar{r}, \bar{r}') = \left[\bar{\bar{I}} + \frac{1}{k^2}\nabla\nabla\right]g(\bar{r}, \bar{r}'). \quad (A7)$$

By substituting Eq. (A7) into Eq. (A6) and after some calculations, we can have

$$g(\bar{r}, \bar{r}') = \frac{e^{ik|\bar{r}-\bar{r}'|}}{4\pi|\bar{r} - \bar{r}'|}. \quad (A8)$$

For a dipolar source with an electric dipole moment of $\bar{p}(\bar{r}')$, we have $\bar{J}(\bar{r}') = \frac{\partial\bar{p}(\bar{r}')}{\partial t}$. By substituting Eqs. (A7) and

(A8) into Eq. (A4), one obtains Eq. (A9):

$$\bar{E}(\bar{r}) = i\omega\mu \left[\bar{\bar{I}} + \frac{1}{k^2}\nabla\nabla \right] \frac{\partial \bar{p}(\bar{r}')}{\partial t} \frac{e^{ikr}}{4\pi r}. \quad (A9)$$

Furthermore, from Eqs. (A1) and (A9), one obtains

$$\bar{H}(\bar{r}) = \nabla \times \frac{\partial \bar{p}(\bar{r}')}{\partial t} \frac{e^{ikr}}{4\pi r}. \quad (A10)$$

From Eqs. (A9) and (A10), we can obtain an exact solution for the total radiation field induced by a source with an electric dipole moment. Without loss of generality, the electric dipole moment can be expressed as $\bar{p}(\bar{r}') = \bar{p} \cdot \delta(\bar{r}')$, and we have $\frac{\partial \bar{p}(\bar{r}')}{\partial t} = -i\omega\bar{p}(\bar{r}')$, where $\bar{p} = \hat{x}p_x + \hat{y}p_y + \hat{z}p_z$.

In order to expand Eqs. (A9) and (A10), we use the Weyl identity, namely,

$$\frac{e^{ikr}}{r} = \frac{i}{2\pi} \iint_{-\infty}^{+\infty} \frac{e^{ik_x x + ik_y y + ik_z|z|}}{k_z} dk_x dk_y, \quad (A11)$$

where $k_z = (k^2 - k_x^2 - k_y^2)^{\frac{1}{2}} = (k^2 - k_\rho^2)^{\frac{1}{2}}$. We denote the angle between $\hat{k}_\rho$ and $\hat{x}$ as α and the angle between $\hat{\rho}$ and $\hat{x}$ as ϕ. Accordingly, $\hat{k}_\rho = \hat{x}k_\rho\cos\alpha + \hat{y}k_\rho\sin\alpha$, $\hat{\rho} = \hat{x}\rho\cos\phi + \hat{y}\rho\sin\phi$, and $dk_x dk_y = k_\rho dk_\rho d\alpha$. Then we have $k_x x + k_y y = k_\rho\rho\cos(\alpha - \phi)$. By substituting the above information into Eq. (A11), Eq. (A11) can be reorganized into

$$\frac{e^{ikr}}{r} = i \int_0^{+\infty} \frac{1}{2\pi} \int_0^{2\pi} e^{ik_\rho\rho\cos(\alpha-\phi)} d\alpha \frac{k_\rho}{k_z} e^{ik_z|z|} dk_\rho. \quad (A12)$$

By applying the integral identity for Bessel functions and the fact that $J_0(k_\rho\rho) = \frac{1}{2}[H_0^{(1)}(k_\rho\rho) + H_0^{(2)}(k_\rho\rho)]$ and $H_0^{(1)}(-k_\rho\rho) = -H_0^{(2)}(k_\rho\rho)$, Eq. (A12) can be reexpressed as

$$\frac{e^{ikr}}{r} = \frac{i}{2} \int_{-\infty}^{+\infty} \frac{k_\rho}{k_z} H_0^{(1)}(k_\rho\rho) e^{ik_z|z|} dk_\rho. \quad (A13)$$

By substituting Eq. (A13) into Eq. (A9), we have the electric field distribution for the electric dipole moment:

$$E_{z,\text{source}}^{\text{electric}}(\rho, \phi, z) = \frac{ip_x}{8\pi\varepsilon} \frac{\partial^2}{\partial x \partial z} \int_{-\infty}^{+\infty} \frac{k_\rho}{k_z} H_0^{(1)}(k_\rho\rho) e^{ik_z|z|} dk_\rho + \frac{ip_y}{8\pi\varepsilon} \frac{\partial^2}{\partial y \partial z} \int_{-\infty}^{+\infty} \frac{k_\rho}{k_z} H_0^{(1)}(k_\rho\rho) e^{ik_z|z|} dk_\rho$$
$$+ \frac{ip_z}{8\pi\varepsilon} \left(k^2 + \frac{\partial^2}{\partial z^2} \right) \int_{-\infty}^{+\infty} \frac{k_\rho}{k_z} H_0^{(1)}(k_\rho\rho) e^{ik_z|z|} dk_\rho. \quad (A14)$$

Since $\frac{\partial H_0^{(1)}(k_\rho\rho)}{\partial x} = -H_1^{(1)}(k_\rho\rho)k_\rho\cos\phi$, $\frac{\partial H_0^{(1)}(k_\rho\rho)}{\partial y} = -H_1^{(1)}(k_\rho\rho)k_\rho\sin\phi$, and $\frac{\partial}{\partial z}e^{ik_z|z|} = ik_z\frac{z}{|z|}e^{ik_z|z|}$, Eq. (A14) can be reduced to

$$E_{z,\text{source}}^{\text{electric}}(\rho, \phi, z) = \frac{ip_x}{8\pi\varepsilon} \int_{-\infty}^{+\infty} -\text{sign}(z)iH_1^{(1)}(k_\rho\rho)k_\rho^2\cos\phi e^{ik_z|z|} dk_\rho + \frac{ip_y}{8\pi\varepsilon} \int_{-\infty}^{+\infty} -\text{sign}(z)iH_1^{(1)}(k_\rho\rho)k_\rho^2\sin\phi e^{ik_z|z|} dk_\rho$$
$$+ \frac{ip_z}{8\pi\varepsilon} \int_{-\infty}^{+\infty} \frac{k_\rho}{k_z} H_0^{(1)}(k_\rho\rho)k_\rho^2 e^{ik_z|z|} dk_\rho. \quad (A15)$$

Under the condition of $H_0^{(1)}(k_\rho\rho) = iH_1^{(1)}(k_\rho\rho)$ with $k_\rho\rho \to \infty$, Eq. (A15) can be reduced to

$$E_{z,\text{source}}^{\text{electric}}(\rho, \phi, z) = \int_{-\infty}^{+\infty} \left(-\frac{1}{8\pi\varepsilon} \left[-\text{sign}(z)(p_x\cos\phi + p_y\sin\phi) + p_z\frac{k_\rho}{k_z} \right] \right) k_\rho^2 H_1^{(1)}(k_\rho\rho) e^{ik_z|z|} dk_\rho. \quad (A16)$$

By substituting Eq. (A13) into Eq. (A10), we have the magnetic field induced by an electric dipole moment $\bar{p} = \hat{x}p_x + \hat{y}p_y + \hat{z}p_z$ as follows:

$$H_{z,\text{source}}^{\text{electric}}(\rho, \phi, z) = \int_{-\infty}^{+\infty} \left[\frac{\omega}{8\pi}(p_x\sin\phi - p_y\cos\phi) \right] \frac{k_\rho^2}{k_z} H_1^{(1)}(k_\rho\rho) e^{ik_z|z|} dk_\rho. \quad (A17)$$

Similarly, we can obtain the field distribution induced by a dipolar source with a magnetic dipole moment $\bar{m}(\bar{r}') = \bar{m} \cdot \delta(\bar{r}')$ through the usage of duality principle $[\bar{E}(\bar{r}) \to \bar{H}(\bar{r}), \bar{H}(\bar{r}) \to -\bar{E}(\bar{r}), \varepsilon \to \mu, \mu \to \varepsilon$, and $\bar{p} \to \mu\bar{m}]$, namely,

$$E_{z,\text{source}}^{\text{magnetic}}(\rho, \phi, z) = \int_{-\infty}^{+\infty} \left[-\frac{\omega\mu}{8\pi}(m_x\sin\phi - m_y\cos\phi) \right] \frac{k_\rho^2}{k_z} H_1^{(1)}(k_\rho\rho) e^{ik_z|z|} dk_\rho, \quad (A18)$$

$$H_{z,\text{source}}^{\text{magnetic}}(\rho, \phi, z) = \int_{-\infty}^{+\infty} \left(-\frac{1}{8\pi} \left[-\text{sign}(z)(m_x\cos\phi + m_y\sin\phi) + m_z\frac{k_\rho}{k_z} \right] \right) k_\rho^2 H_1^{(1)}(k_\rho\rho) e^{ik_z|z|} dk_\rho. \quad (A19)$$

Then, we can get the total field induced by a dipolar source with an electric dipole moment $\bar{p}$ and a magnetic dipole moment $\bar{m}$ as follows:

$$E_{z,\text{source}}(\rho, \phi, z) = E_{z,\text{source}}^{\text{electric}}(\rho, \phi, z) + E_{z,\text{source}}^{\text{magnetic}}(\rho, \phi, z), \quad (A20)$$

$$H_{z,\text{source}}(\rho, \phi, z) = H_{z,\text{source}}^{\text{electric}}(\rho, \phi, z) + H_{z,\text{source}}^{\text{magnetic}}(\rho, \phi, z). \quad (A21)$$

lower radiation pattern of
excited surface wave at z=-d

upper radiation pattern of
excited surface wave at z=d

twist angle between the lower
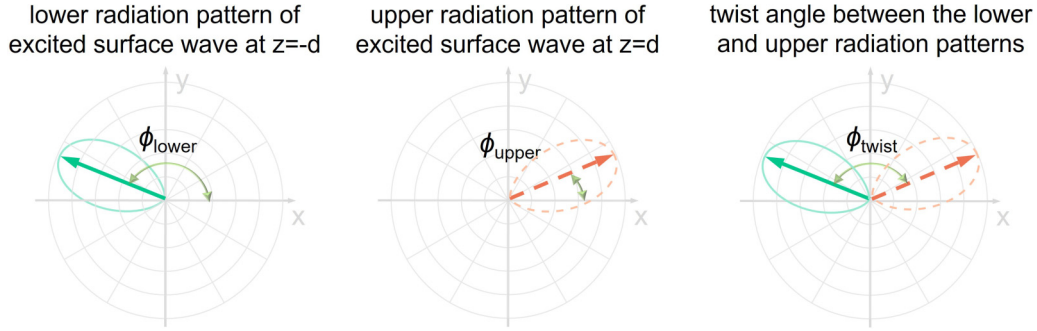and upper radiation patterns

FIG. 5. Conceptual illustration of the twist angle with $\phi_{\text{lower}} > \phi_{\text{upper}}$. Here, the upper and lower near-field radiation patterns are calculated by using $|D^{\text{upper}}_{z,\text{sw},z=d}(\phi)|$ and $|D^{\text{lower}}_{z,\text{sw},z=-d}(\phi)|$ of the induced surface waves in the upper and lower interfaces at $z = d$ and $z = -d$, respectively. These radiation patterns have the same shape but have the feature of an oriented misalignment, namely, $|D^{\text{upper}}_{z,\text{sw},z=d}(\phi)| = |D^{\text{lower}}_{z,\text{sw},z=-d}(\phi - \phi_{\text{twist}})|$ or $|D^{\text{upper}}_{z,\text{sw},z=d}(\phi)| = |D^{\text{lower}}_{z,\text{sw},z=-d}(\phi + \phi_{\text{twist}})|$. The definition of ϕ_{twist} is schematically provided in the plot, which is always within the range of $0° - 180°$.

APPENDIX B: MORE SCHEMATIC ILLUSTRATION OF THE TWIST ANGLE

According to the definition of twist angle in Eq. (4) in the main text, the twist angle is always within the range of $0° - 180°$. For clarity, we provide two cases of the definition of the twist angle in Figs. 5 and 6.

APPENDIX C: EXCITED SURFACE WAVES WHEN THE DIPOLAR SOURCE IS BELOW THE OUTCOUPLER

In this Appendix, we investigate three cases of near-field dipolar radiation, including the case having the source located below the outcoupler in Fig. 7(a), the case having the source located above the outcoupler in Fig. 7(b), and the case having the source located in the middle of two outcouplers in Fig. 7(c).

In this section, we calculate the excited surface waves if the dipolar source is below the outcoupler in Fig. 7(a). Consider that the dipolar source is at $z = 0$ and the outcoupler is at $z = d$ $(d > 0)$ as shown in Fig. 5(a). The field above (below) the dipolar source is denoted as $E^{\text{upgoing(downgoing)}}_{z,\text{source}}$. The regions above and below the outcoupler are denoted as region 1 and region 2, respectively. The relative permittivity in region 1 and region 2 is ε_{r1} and ε_{r2}, respectively. The relative permeability in region 1 and region 2 is μ_{r1} and μ_{r2}, respectively. Below we first calculate the field distribution in region 1, namely,

$$E_{1z}(\rho, \phi, z) = \int_{-\infty}^{+\infty} E^{\text{upgoing}}_{z,\text{source}}(k_\rho, \phi) H_1^{(1)}(k_\rho \rho) T^{\text{TM}}_{21} e^{i(k_{2z} - k_{1z})d} e^{ik_{1z}z} dk_\rho. \tag{C1}$$

Region 2 can be divided into two parts with $0 < z < d$ and $z < 0$. For $0 < z < d$, the total field for E_z can be expressed as

$$E^{0<z<d}_{2z}(\rho, \phi, z) = \int_{-\infty}^{+\infty} E^{\text{upgoing}}_{z,\text{source}}(k_\rho, \phi) \left[e^{ik_{2z}z} + R^{\text{TM}}_{21} e^{2ik_{2z}d} e^{-ik_{2z}z} \right] H_1^{(1)}(k_\rho \rho) dk_\rho. \tag{C2}$$

For $z < 0$, the total field for E_z can be expressed as

$$E^{z<0}_{2z}(\rho, \phi, z) = \int_{-\infty}^{+\infty} \left[E^{\text{downgoing}}_{z,\text{source}}(k_\rho, \phi) + E^{\text{upgoing}}_{z,\text{source}}(k_\rho, \phi) R^{\text{TM}}_{21} e^{2ik_{2z}d} \right] H_1^{(1)}(k_\rho \rho) e^{-ik_{2z}z} dk_\rho. \tag{C3}$$

lower radiation pattern of
excited surface wave at z=-d

upper radiation pattern of
excited surface wave at z=d

twist angle between the lower
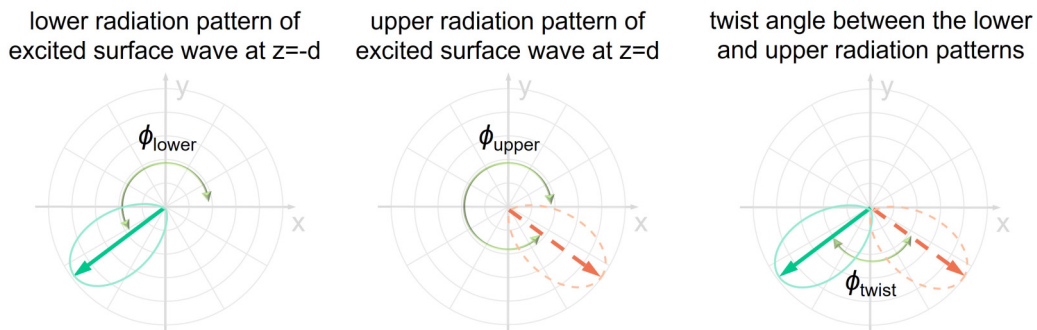and upper radiation patterns

FIG. 6. Conceptual illustration of the twist angle with $\phi_{\text{lower}} < \phi_{\text{upper}}$. The twist angle is schematically defined in the plot and is always within the range of $0° - 180°$.
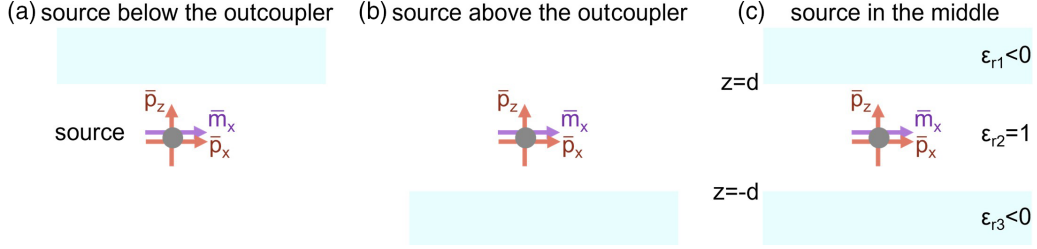
FIG. 7. Structural schematic of dipolar radiation. For illustration, each outcoupler supports the propagation of TM surface waves and can be constructed, for example, by the optical interface between vacuum and a negative-permittivity material (e.g., metal). (a) The dipolar source is located below the designed interface. (b) The dipolar source is located above the designed interface. (c) The dipolar source is located in the middle of two parallel outcouplers.

In the above equations, $T_{21}^{\mathrm{TM}} = \frac{2\varepsilon_2 k_{2z}}{\varepsilon_1 k_{2z}+\varepsilon_2 k_{2z}}$ is the transmission coefficient, and $R_{21}^{\mathrm{TM}} = \frac{\varepsilon_1 k_{2z}-\varepsilon_2 k_{1z}}{\varepsilon_1 k_{2z}+\varepsilon_2 k_{1z}}$ is the reflection coefficient.

When the dipolar source is composed of an electric dipole moment $\bar{p} = \hat{z}p_z + \hat{x}p_x$ and a magnetic dipole moment $\bar{m} = \hat{x}m_x$, Eq. (C3) can be reduced to

$$E_{1z}(\rho, \phi, z) = \int_{-\infty}^{+\infty} E_{z,\mathrm{source}}^{\mathrm{upgoing}}(k_\rho, \phi) H_1^{(1)}(k_\rho\rho) T_{21}^{\mathrm{TM}} e^{i(k_{2z}-k_{1z})d} e^{ik_{1z}z} dk_\rho, \tag{C4}$$

where

$$E_{z,\mathrm{source}}^{\mathrm{upgoing}}(k_\rho, \phi) = \left[-\frac{1}{8\pi\varepsilon_2}\left(-p_x\cos\phi + p_z\frac{k_\rho}{k_{2z}}\right) - \frac{\omega\mu_2}{8\pi}m_x\frac{\sin\phi}{k_{2z}}\right]k_\rho^2. \tag{C5}$$

By applying the plasmon pole approximation for the integration of k_ρ in Eq. (C4), the excited field of the surface wave at the upper interface at $z = d$ has

$$E_{1z,\mathrm{sw}}^{\mathrm{upper}}(\rho, \phi, z = d) \approx 2\pi i \mathrm{Res}\left[E_{z,\mathrm{source}}^{\mathrm{upgoing}}(k_\rho, \phi) H_1^{(1)}(k_\rho\rho) T_{21}^{\mathrm{TM}} e^{ik_{2z}d}, k_\rho = k_{\rho,\mathrm{sw}}\right]$$

$$= 2\pi i E_{z,\mathrm{source}}^{\mathrm{upgoing}}(k_{\rho,\mathrm{sw}}, \phi) H_1^{(1)}(k_{\rho,\mathrm{sw}}\rho) e^{ik_{2z,\mathrm{sw}}d} \mathrm{Res}\left[T_{21}^{\mathrm{TM}}, k_\rho = k_{\rho,\mathrm{sw}}\right], \tag{C6}$$

where $\bar{k}_{\mathrm{sw}} = \hat{\rho}k_{\rho,\mathrm{sw}} + \hat{z}k_{z,\mathrm{sw}}$ is the wave vector of excited surface waves. When $\sqrt{1 + \left(\frac{k_0}{k_{2z,\mathrm{sw}}}\frac{m_x/c}{p_x}\right)^2} \neq 0$, where $k_{2z,\mathrm{sw}} = \sqrt{k_2^2-k_{\rho,\mathrm{sw}}^2}$, $k_2^2 = \varepsilon_{r2}\mu_{r2}k_0^2$, $k_0 = \omega/c$, ω is the angular frequency, and c is the speed of light in free space. Then Eq. (C6) can be reduced to

$$D_{1z,\mathrm{sw}}^{\mathrm{upper}}(\phi) = E_0\varepsilon_1 p_x\sqrt{1 + \left(\frac{k_0}{k_{2z,\mathrm{sw}}}\frac{m_x/c}{p_x}\right)^2}\left[\sin(\phi + \phi_0) + \frac{\frac{k_{\rho,\mathrm{sw}}}{k_{2z,\mathrm{sw}}}\frac{p_z}{p_x}}{\sqrt{1 + \left(\frac{k_0}{k_{2z,\mathrm{sw}}}\frac{m_x/c}{p_x}\right)^2}}\right], \tag{C7}$$

where $E_0 = 2\pi i \mathrm{Res}[T_{21}^{\mathrm{TM}}, k_\rho = k_{\rho,\mathrm{sw}}]k_{\rho,\mathrm{sw}}^2 e^{ik_{2z,\mathrm{sw}}d} H_1^{(1)}(k_{\rho,\mathrm{sw}}\rho)\frac{-1}{8\pi\varepsilon_2}$, $\sin(\phi_0) = \frac{-1}{\sqrt{1+\left(\frac{k_0}{k_{2z,\mathrm{sw}}}\frac{m_x/c}{p_x}\right)^2}}$, $\cos(\phi_0) = \frac{\frac{k_0}{k_{2z,\mathrm{sw}}}\frac{m_x/c}{p_x}}{\sqrt{1+\left(\frac{k_0}{k_{2z,\mathrm{sw}}}\frac{m_x/c}{p_x}\right)^2}}$, $\phi_0 = 90° - \arctan\left(-\frac{k_0}{k_{2z,\mathrm{sw}}}\frac{m_x/c}{p_x}\right) + m \times 180°$, where $m = 0$ or 1 to ensure $\phi_0 \in [0°, 360°]$. Here, the matter for region 2 is vacuum, and $k_{2z,\mathrm{sw}}$ is reexpressed as $k_{z,\mathrm{sw}}$ in the main text. If $\sqrt{1 + \left(\frac{k_0}{k_{2z,\mathrm{sw}}}\frac{m_x/c}{p_x}\right)^2} = 0$, the relevant discussion is provided in Appendix F.

As an example, we show in Fig. 8 the field distribution of excited TM surface waves at the interface of $z = d$ with different values of ϕ_{upper}.

APPENDIX D: EXCITED SURFACE WAVES WHEN THE DIPOLAR SOURCE IS ABOVE THE OUTCOUPLER

In this section, we calculate the field distribution when the outcoupler is placed below the dipolar source in Fig. 7(b). The dipolar source is at $z = 0$ and the outcoupler is at $z = -d$ as shown in Fig. 5(b). The region above the outcoupler is denoted as region 2. The region below the outcoupler is denoted as region 3. The relative permittivity in region 2 and region 3 is ε_{r2} and ε_{r3}, respectively. The relative permeability in region 2 and region 3 is μ_{r2} and μ_{r3}, respectively. For region 3 with $z < -d$, the total fields of E_z can be expressed as

$$E_{3z}(\rho, \phi, z) = \int_{-\infty}^{+\infty} E_{z,\mathrm{source}}^{\mathrm{downgoing}}(k_\rho, \phi) H_1^{(1)}(k_\rho\rho) T_{23}^{\mathrm{TM}} e^{i(k_{2z}-k_{3z})d} e^{-ik_{3z}z} dk_\rho. \tag{D1}$$
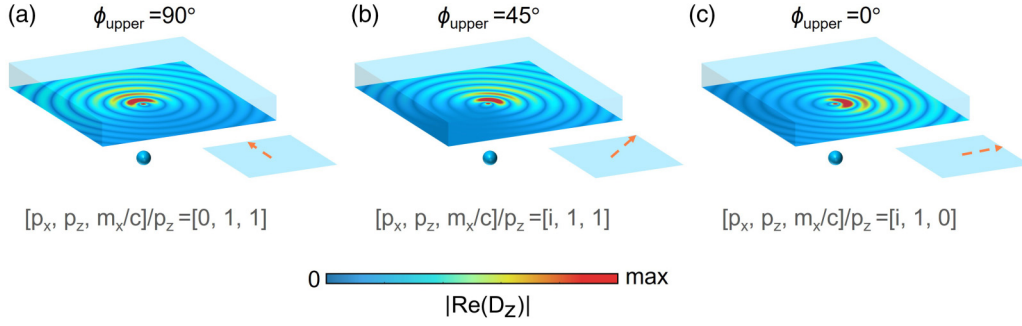
FIG. 8. Field distribution of excited TM surface waves at the interface of $z = d$. The structural setup is the same as Fig. 5(a) with the use of $\varepsilon_{r1} = -2$. (a) $\phi_{\mathrm{upper}} = 90°$, if the dipolar source is constructed by $[p_x, p_z, m_x/c]/p_z = [0, 1, 1]$. (b) $\phi_{\mathrm{upper}} = 45°$, if the dipolar source is constructed by $[p_x, p_z, m_x/c]/p_z = [i, 1, 1]$. (c) $\phi_{\mathrm{upper}} = 0°$, if the dipolar source is composed of $[p_x, p_z, m_x/c]/p_z = [i, 1, 0]$.

Region 2 can be divided into two parts with $-d < z < 0$ and $z > 0$, For the part with $-d < z < 0$, the total field of E_z can be expressed as

$$E_{2z}^{-d<z<0}(\rho, \phi, z) = \int_{-\infty}^{+\infty} E_{z,\mathrm{source}}^{\mathrm{downgoing}}(k_\rho, \phi)\left[e^{-ik_{2z}z} + R_{21}^{\mathrm{TM}}e^{2ik_{2z}d}e^{ik_{2z}z}\right]H_1^{(1)}(k_\rho\rho)dk_\rho. \tag{D2}$$

For the part with $z > 0$, the total field of E_z can be expressed as

$$E_{2z}^{z>0}(\rho, \phi, z) = \int_{-\infty}^{+\infty} \left[E_{z,\mathrm{source}}^{\mathrm{upgoing}}(k_\rho, \phi) + E_{z,\mathrm{source}}^{\mathrm{downgoing}}(k_\rho, \phi)R_{23}^{\mathrm{TM}}e^{2ik_{2z}d}\right]e^{ik_{2z}z}H_1^{(1)}(k_\rho\rho)dk_\rho. \tag{D3}$$

In the above equations, $T_{23}^{\mathrm{TM}} = \frac{2\varepsilon_2 k_{2z}}{\varepsilon_3 k_{2z} + \varepsilon_2 k_{3z}}$ is the transmission coefficient, and $R_{23}^{\mathrm{TM}} = \frac{\varepsilon_3 k_{2z} - \varepsilon_2 k_{3z}}{\varepsilon_3 k_{2z} + \varepsilon_2 k_{3z}}$ is the reflection coefficient $R_{23}^{\mathrm{TM}} = \frac{\varepsilon_3 k_{2z} - \varepsilon_2 k_{3z}}{\varepsilon_3 k_{2z} + \varepsilon_2 k_{3z}}$.

For the outcoupler below the source, similarly, we have

$$E_{z,\mathrm{source}}^{\mathrm{downgoing}}(k_\rho, \phi) = \left[-\frac{1}{8\pi\varepsilon_2}\left(+p_x\cos\phi + p_z\frac{k_\rho}{k_{2z}}\right) - \frac{\omega\mu_2}{8\pi}m_x\frac{\sin\phi}{k_{2z}}\right]k_\rho^2, \tag{D4}$$

$$E_{3z,\mathrm{sw}}^{\mathrm{lower}}(\rho, \phi, z = -d) \approx 2\pi i\mathrm{Res}\left[E_{z,\mathrm{source}}^{\mathrm{downgoing}}(k_\rho, \phi)H_1^{(1)}(k_\rho\rho)T_{23}^{\mathrm{TM}}e^{ik_{2z}d}, k_\rho = k_{\rho,\mathrm{sw}}\right]$$
$$= 2\pi i E_{z,\mathrm{source}}^{\mathrm{downgoing}}(k_{\rho,\mathrm{sw}}, \phi)H_1^{(1)}(k_{\rho,\mathrm{sw}}\rho)e^{ik_{2z,\mathrm{sw}}d}\mathrm{Res}\left[T_{23}^{\mathrm{TM}}, k_\rho = k_{\rho,\mathrm{sw}}\right], \tag{D5}$$

$$D_{3z,\mathrm{sw}}^{\mathrm{lower}}(\phi) = E_0\varepsilon_3 p_x\sqrt{1 + \left(\frac{k_0}{k_{2z,\mathrm{sw}}}\frac{m_x/c}{p_x}\right)^2}\left[\sin(\phi - \phi_0) + \frac{\frac{k_{\rho,\mathrm{sw}}}{k_{2z,\mathrm{sw}}}\frac{p_z}{p_x}}{\sqrt{1 + \left(\frac{k_0}{k_{2z,\mathrm{sw}}}\frac{m_x}{c}\frac{1}{p_x}\right)^2}}\right]. \tag{D6}$$

For example, we show in Fig. 9 the field distribution of excited TM surface waves at the interface of $z = -d$ with different values of ϕ_{lower}.
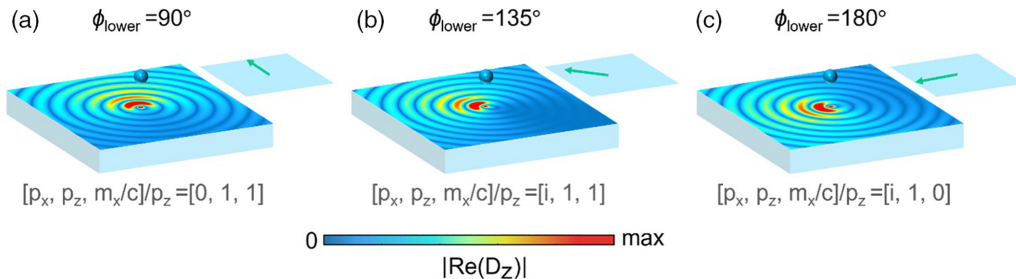

FIG. 9. Field distribution of excited TM surface waves at the interface of $z = -d$. The structural setup is the same as Fig. 5(b) with the use of $\varepsilon_{r3} = -2$. (a) $\phi_{\mathrm{lower}} = 90°$, if the dipolar source is constructed by $[p_x, p_z, m_x/c]/p_z = [0, 1, 1]$. (b) $\phi_{\mathrm{lower}} = 135°$, if the dipolar source is constructed by $[p_x, p_z, m_x/c]/p_z = [i, 1, 1]$. (c) $\phi_{\mathrm{lower}} = 180°$, if the dipolar source is composed of $[p_x, p_z, m_x/c]/p_z = [i, 1, 0]$.

APPENDIX E: EXCITED SURFACE WAVES WHEN THE DIPOLAR SOURCE IS IN THE MIDDLE OF TWO OUTCOUPLERS

In this section we give the detailed derivation of excited TM surface waves, if the dipolar source is in the middle of two outcouplers in Fig. 7(c). We define that the upper interface is at $z = d$ ($d > 0$), and the lower interface is at $z = -d$ as shown in Fig. 5(c). Regions of $z > d$, $-d < z < d$, and $z < -d$ are denoted as regions 1, 2, and 3, respectively. The relative permittivity in regions 1, 2, and 3 are ε_{r1}, ε_{r2}, and ε_{r3}, respectively. Then we first calculate the E_z field distribution inside region 2. The field above (below) the dipolar source is denoted as $E_{z,\text{source}}^{\text{upgoing(downgoing)}}$.

For $0 < z < d$ in region 2, the total field of E_z can be expressed as

$$E_{2z,0<z<d}^{\text{upgoing}} e^{ik_{2z}z} = E_{z,\text{source}}^{\text{upgoing}} e^{ik_{2z}z} + E_{2z,-d<z<0}^{\text{downgoing}} R_{23}^{\text{TM}} e^{2ik_{2z}d} e^{ik_{2z}z}, \quad \text{(E1)}$$

$$E_{2z,0<z<d}^{\text{downgoing}} e^{-ik_{2z}z} = E_{2z,0<z<d}^{\text{upgoing}} R_{21}^{\text{TM}} e^{2ik_{2z}d} e^{-ik_{2z}z}. \quad \text{(E2)}$$

For $-d < z < 0$ in region 2, the total field of E_z can be expressed as

$$E_{2z,-d<z<0}^{\text{upgoing}} e^{ik_{2z}z} = E_{2z,-d<z<0}^{\text{downgoing}} R_{23}^{\text{TM}} e^{2ik_{2z}d} e^{ik_{2z}z}, \quad \text{(E3)}$$

$$E_{2z,-d<z<0}^{\text{downgoing}} e^{-ik_{2z}z} = E_{z,\text{source}}^{\text{downgoing}} e^{-ik_{2z}z} + E_{2z,0<z<d}^{\text{upgoing}} R_{21}^{\text{TM}} e^{2ik_{2z}d} e^{-ik_{2z}z}. \quad \text{(E4)}$$

On the basis of Eqs. (E1)–(E4), we have the E_z total field in region 2 as follows:

$$E_{2z,0<z<d}^{\text{upgoing}}(k_\rho,\phi)$$
$$= \frac{E_{z,\text{source}}^{\text{upgoing}}(k_\rho,\phi) + E_{z,\text{source}}^{\text{downgoing}}(k_\rho,\phi) R_{23}^{\text{TM}} e^{2ik_{2z}d}}{1 - R_{21}^{\text{TM}} e^{2ik_{2z}d} R_{23}^{\text{TM}} e^{2ik_{2z}d}}, \quad \text{(E5)}$$

$$E_{2z,-d<z<0}^{\text{upgoing}}(k_\rho,\phi) = \frac{E_{z,\text{source}}^{\text{downgoing}}(k_\rho,\phi) R_{23}^{\text{TM}} e^{2ik_{2z}d}}{1 - R_{21}^{\text{TM}} e^{2ik_{2z}d} R_{23}^{\text{TM}} e^{2ik_{2z}d}}, \quad \text{(E6)}$$

$$E_{2z,0<z<d}^{\text{downgoing}}(k_\rho,\phi) = \frac{E_{z,\text{source}}^{\text{upgoing}}(k_\rho,\phi) R_{21}^{\text{TM}} e^{2ik_{2z}d}}{1 - R_{21}^{\text{TM}} e^{2ik_{2z}d} R_{23}^{\text{TM}} e^{2ik_{2z}d}}, \quad \text{(E7)}$$

$$E_{2z,-d<z<0}^{\text{downgoing}}(k_\rho,\phi)$$
$$= \frac{E_{z,\text{source}}^{\text{downgoing}}(k_\rho,\phi) + E_{z,\text{source}}^{\text{upgoing}}(k_\rho,\phi) R_{21}^{\text{TM}} e^{2ik_{2z}d}}{1 - R_{21}^{\text{TM}} e^{2ik_{2z}d} R_{23}^{\text{TM}} e^{2ik_{2z}d}}. \quad \text{(E8)}$$

In the above equations, $R_{21}^{\text{TM}} = \frac{\varepsilon_1 k_{2z} - \varepsilon_2 k_{1z}}{\varepsilon_1 k_{2z} + \varepsilon_2 k_{1z}}$ and $R_{23}^{\text{TM}} = \frac{\varepsilon_3 k_{2z} - \varepsilon_2 k_{3z}}{\varepsilon_3 k_{2z} + \varepsilon_2 k_{3z}}$ are the reflection coefficients.

Now we turn to calculating the field distribution in region 1 and region 3. For region 1, the total fields of E_z can be expressed as

$$E_{1z}(\rho,\phi,z) = \int_{-\infty}^{+\infty} E_{2z,0<z<d}^{\text{upgoing}}(k_\rho,\phi) H_1^{(1)}(k_\rho\rho) T_{21}^{\text{TM}}$$
$$\times e^{i(k_{2z}-k_{1z})d} e^{ik_{1z}z} dk_\rho. \quad \text{(E9)}$$

For region 3, the total field of E_z can be expressed as

$$E_{3z}(\rho,\phi,z) = \int_{-\infty}^{+\infty} E_{2z,-d<z<0}^{\text{downgoing}}(k_\rho,\phi) H_1^{(1)}(k_\rho\rho) T_{23}^{\text{TM}}$$
$$\times e^{i(k_{2z}-k_{3z})d} e^{-ik_{3z}z} dk_\rho. \quad \text{(E10)}$$

In the above equations, $T_{21}^{\text{TM}} = T_{23}^{\text{TM}} = \frac{2\varepsilon_2 k_{2z}}{\varepsilon_3 k_{2z} + \varepsilon_2 k_{3z}}$ is the transmission coefficient.

Under the condition of $\varepsilon_{r1} = \varepsilon_{r3}$ (namely, regions 1 and 3 are the same), we have $R_{21}^{\text{TM}} = R_{23}^{\text{TM}} = \frac{A}{B}$, $T_{21}^{\text{TM}} = \frac{C}{B}$, $A = \varepsilon_1 k_{2z} - \varepsilon_2 k_{1z}$, $B = \varepsilon_1 k_{2z} + \varepsilon_2 k_{1z}$, and $C = 2\varepsilon_2 k_{2z}$. These above equations (E5) and (E8)–(E10) can then be reduced to

$$E_{2z,0<z<d}^{\text{upgoing}}(k_\rho,\phi)$$
$$= \frac{E_{z,\text{source}}^{\text{upgoing}}(k_\rho,\phi)B + E_{z,\text{source}}^{\text{downgoing}}(k_\rho,\phi)A e^{2ik_{2z}d}}{(B - A e^{2ik_{2z}d})(B + A e^{2ik_{2z}d})}, \quad \text{(E11)}$$

$$E_{1z}(\rho,\phi,z) = \int_{-\infty}^{+\infty} E_{2z,0<z<d}^{\text{upgoing}}(k_\rho,\phi) H_1^{(1)}(k_\rho\rho) T_{21}^{\text{TM}}$$
$$\times e^{i(k_{2z}-k_{1z})d} e^{ik_{1z}z} dk_\rho, \quad \text{(E12)}$$

$$E_{2z,-d<z<0}^{\text{downgoing}}(k_\rho,\phi)$$
$$= \frac{E_{z,\text{source}}^{\text{downgoing}}(k_\rho,\phi)B + E_{z,\text{source}}^{\text{upgoing}}(k_\rho,\phi)A e^{2ik_{2z}d}}{(B - A e^{2ik_{2z}d})(B + A e^{2ik_{2z}d})}, \quad \text{(E13)}$$

$$E_{3z}(\rho,\phi,z) = \int_{-\infty}^{+\infty} E_{2z,-d<z<0}^{\text{downgoing}}(k_\rho,\phi) H_1^{(1)}(k_\rho\rho) T_{21}^{\text{TM}}$$
$$\times e^{i(k_{2z}-k_{1z})d} e^{-ik_{1z}z} dk_\rho. \quad \text{(E14)}$$

By applying the plasmon pole approximation for the integration of k_ρ in Eqs. (E12) and (E14), these equations can be reduced to

$$E_{1z,\text{sw}}^{\text{upper}}(\rho,\phi,z=d) \approx 2\pi i \text{Res} \sum_{k_{\rho,\text{sw1}}}^{k_{\rho,\text{sw3}}} \left[E_{z2,0<z<d}^{\text{upgoing}}(k_\rho,\phi) H_1^{(1)} \right.$$
$$\left. \times (k_\rho\rho) T_{21}^{\text{TM}} e^{ik_{2z}d}, k_\rho = k_{\rho,\text{sw}i} \right], \quad \text{(E15)}$$

$$E_{3z,\text{sw}}^{\text{lower}}(\rho,\phi,z=-d) \approx 2\pi i \text{Res} \sum_{k_{\rho,\text{sw1}}}^{k_{\rho,\text{sw3}}} \left[E_{z2,-d<z<0}^{\text{downgoing}}(k_\rho,\phi) H_1^{(1)} \right.$$
$$\left. \times (k_\rho\rho) T_{21}^{\text{TM}} e^{ik_{2z}d}, k_\rho = k_{\rho,\text{sw}i} \right], \quad \text{(E16)}$$

where $\bar{k}_{\text{sw1}} = \hat{\rho} k_{\rho,\text{sw1}} + \hat{z} k_{z,\text{sw1}}$ and $\bar{k}_{\text{sw3}} = \hat{\rho} k_{\rho,\text{sw3}} + \hat{z} k_{z,\text{sw3}}$ are the wave vectors of excited surface waves in regions 1 and 3, respectively. For simplicity, here we define

$$\beta_{\text{sw}i} = \text{Res}\left[\frac{1}{B^2 - A^2 e^{4ik_{2z}d}}, k_\rho = k_{\rho,\text{sw}i} \right] H_1^{(1)}(k_{\rho,\text{sw}i}\rho)$$
$$\times C_{\text{sw}i} e^{ik_{z,\text{sw}i}d}, \quad \text{(E17)}$$

where $k_{2z,\text{sw}i} = \sqrt{k_2^2 - k_{\rho,\text{sw}i}^2}$, $C_{\text{sw}i} = 2\varepsilon_2 k_{2z,\text{sw}i}$.
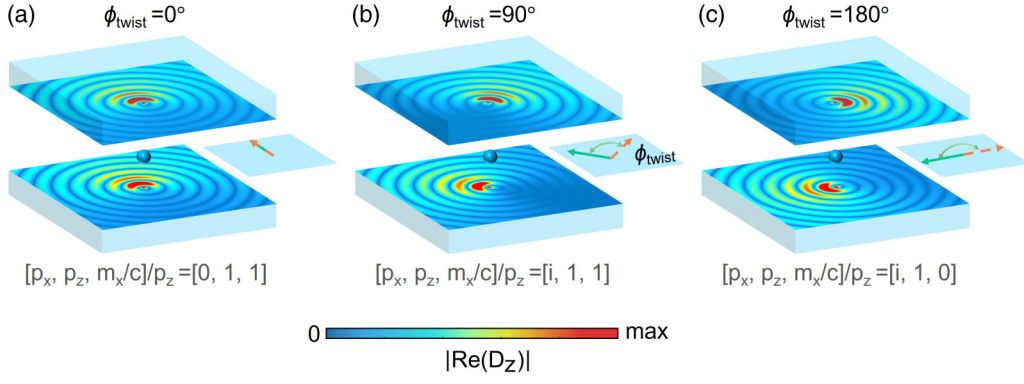
FIG. 10. Field distribution of Janus faces of dipolar sources in directional near-field coupling with an oriented misalignment. The structural setup is the same as Fig. 5(c) with the use of $\varepsilon_{r1} = \varepsilon_{r3} = -2$. (a) $\phi_{\text{twist}} = 0°$, if the dipolar source is constructed by $[p_x, p_z, m_x/c]/p_z = [0, 1, 1]$. (b) $\phi_{\text{twist}} = 90°$, if the dipolar source is constructed by $[p_x, p_z, m_x/c]/p_z = [i, 1, 1]$. (c) $\phi_{\text{twist}} = 180°$, if the dipolar source is composed of $[p_x, p_z, m_x/c]/p_z = [i, 1, 0]$.

With the application of Eqs. (E17), Eqs. (E15) and (E16) can be reduced to

$$D_{1z,\text{sw}}^{\text{upper}}(\rho, \phi, z = d) \approx 2\pi i \sum_{i=1}^{i=3}[\beta_{\text{swi}} m_{1,\text{swi}}]\varepsilon_1, \qquad \text{(E18)}$$

$$D_{3z,\text{sw}}^{\text{lower}}(\rho, \phi, z = -d) \approx 2\pi i \sum_{i=1}^{i=3}[\beta_{\text{swi}} m_{3,\text{swi}}]\varepsilon_3. \qquad \text{(E19)}$$

In Eqs. (E18) and (E19), the factors $m_{1,\text{swi}}$ and $m_{3,\text{swi}}$ are defined as

$$m_{1,\text{swi}} = E_{z,\text{source}}^{\text{upgoing}}(k_{\rho,\text{swi}}, \phi)B_{\text{swi}}$$
$$+ E_{z,\text{source}}^{\text{downgoing}}(k_{\rho,\text{swi}}, \phi)A_{\text{swi}}e^{2ik_{2z,\text{swi}}d}, \qquad \text{(E20)}$$

$$m_{3,\text{swi}} = E_{z,\text{source}}^{\text{downgoing}}(k_{\rho,\text{swi}}, \phi)B_{\text{swi}}$$
$$+ E_{z,\text{source}}^{\text{upgoing}}(k_{\rho,\text{swi}}, \phi)A_{\text{swi}}e^{2ik_{2z,\text{swi}}d}, \qquad \text{(E21)}$$
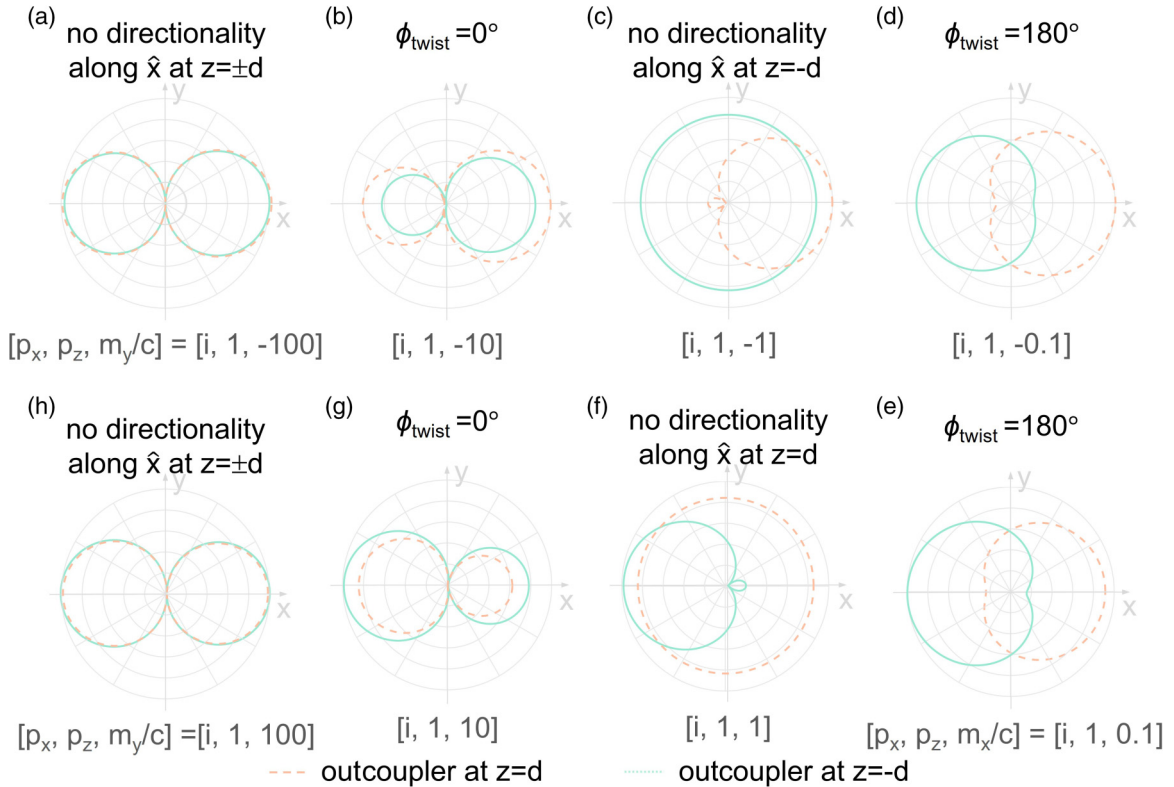

FIG. 11. Upper and lower near-field radiation patterns of a dipolar source with $[p_x, p_z, m_y/c] = [i, 1, b_m]$. The structural setup is the same as Fig. 1, except for the dipolar component of the source. (a) $b_m = -100$. (b) $b_m = -10$. (c) $b_m = -1$. (d) $b_m = -0.1$. (e) $b_m = 0.1$. (f) $b_m = 1$. (g) $b_m = 10$. (h) $b_m = 100$.

where $A_{\text{swi}} = \varepsilon_1 k_{2z,\text{swi}} - \varepsilon_2 k_{1z,\text{swi}}$, and $B_{\text{swi}} = \varepsilon_1 k_{2z,\text{swi}} + \varepsilon_2 k_{1z,\text{swi}}$.

As an example, we show in Fig. 10 the field distribution of Janus faces of dipolar sources in directional near-field coupling with different values of ϕ_{twist}.

APPENDIX F: DEFINITION OF THE TWIST ANGLE WHEN $\sqrt{1 + (\frac{k_0}{k_{z,\text{sw}}} \frac{m_x/c}{p_x})^2} = 0$

This section serves as the complementary information for Eqs. (1) and (3) in the main text.

If the outcoupler locates at the upper side of the source (Appendix D), the field distribution of excited TM surface waves can be expressed as

$$D_{z,\text{sw},z=d}^{\text{upper}}(\phi) = D_1 \left[\frac{k_0}{k_{z,\text{sw}}} \frac{m_x}{c} \sin\phi - p_x \cos\phi + \frac{k_{\rho,\text{sw}}}{k_{z,\text{sw}}} p_z \right],$$

(F1)

where $D_1 = 2\pi i \text{Res}[T_{21}^{\text{TM}}, k_\rho = k_{\rho,\text{sw}}] k_{\rho,\text{sw}}^2 e^{ik_{z,\text{sw}}d} H_1^{(1)}(k_{\rho,\text{sw}}\rho) \frac{1}{4\pi}$. In the main text, we discuss the case with $\sqrt{1 + (\frac{k_0}{k_{z,\text{sw}}} \frac{m_x/c}{p_x})^2} \neq 0$. Below we discuss the case with $\sqrt{1 + (\frac{k_0}{k_{z,\text{sw}}} \frac{m_x/c}{p_x})^2} = 0$.

When $\sqrt{1 + (\frac{k_0}{k_{z,\text{sw}}} \frac{m_x/c}{p_x})^2} = 0$ (namely, $\frac{k_0}{k_{z,\text{sw}}} \frac{m_x/c}{p_x} = \pm i$), by using Euler's formula, Eq. (56) can be reexpressed as

$$D_{z,\text{sw},z=d}^{\text{upper}}(\phi) = D_1(-p_x) \left[e^{i(\frac{ik_0}{k_{z,\text{sw}}} \frac{m_x/c}{p_x})\phi} + \left(-\frac{k_{\rho,\text{sw}}}{k_{z,\text{sw}}} \frac{p_z}{p_x} \right) \right].$$

(F2)

The near-field radiation patterns are calculated by using $|D_{z,\text{sw},z=d}^{\text{upper}}(\phi)|$ of the excited surface waves on the upper interfaces, and the angular direction with the maximum radiation has $|D_{z,\text{sw},z=d}^{\text{upper}}(\phi = \phi_{\text{max}}^{\text{upper}})| = \max[|D_{z,\text{sw},z=d}^{\text{upper}}(\phi)|]$. $|\frac{k_{\rho,\text{sw}}}{k_{z,\text{sw}}} \frac{p_z}{p_x}|$ should be close to 1, in order to make the field of $D_{z,\text{sw},z=d}^{\text{upper}}(\phi)$ highly asymmetric with respect to ϕ, namely, $|\frac{D_{z,\text{sw},z=d}^{\text{upper}}(\phi=\phi_{\text{max}}^{\text{upper}})}{D_{z,\text{sw},z=d}^{\text{upper}}(\phi=\phi_{\text{max}}^{\text{upper}}+180°)}| \gg 1$, where

$$\left(\frac{ik_0}{k_{z,\text{sw}}} \frac{m_x/c}{p_x} \right) \phi_{\text{max}}^{\text{upper}} = \arg\left(-\frac{k_{\rho,\text{sw}}}{k_{z,\text{sw}}} \frac{p_z}{p_x} \right) + 2m_{\text{upper}}\pi, \quad \text{(F3)}$$

where m_{upper} is an integer to ensure $\phi_{\text{max}}^{\text{upper}} \in [0°, 360°]$.

If the outcoupler locates at the lower side of the source, we have the field distribution of excited TM surface waves expressed as

$$D_{z,\text{sw},z=d}^{\text{upper}}(\phi) = D_1 \left[\frac{k_0}{k_{z,\text{sw}}} \frac{m_x}{c} \sin\phi + p_x \cos\phi + \frac{k_{\rho,\text{sw}}}{k_{z,\text{sw}}} p_z \right].$$

(F4)

(a) dipolar source in vacuum (without outcouplers at z=±d)

(b)

(c) dipolar source in a three-layer structure (with outcouplers at z=±d)

(d)

$[p_x, p_z, m_x/c]/p_z = [0.42i, 1, 1]$
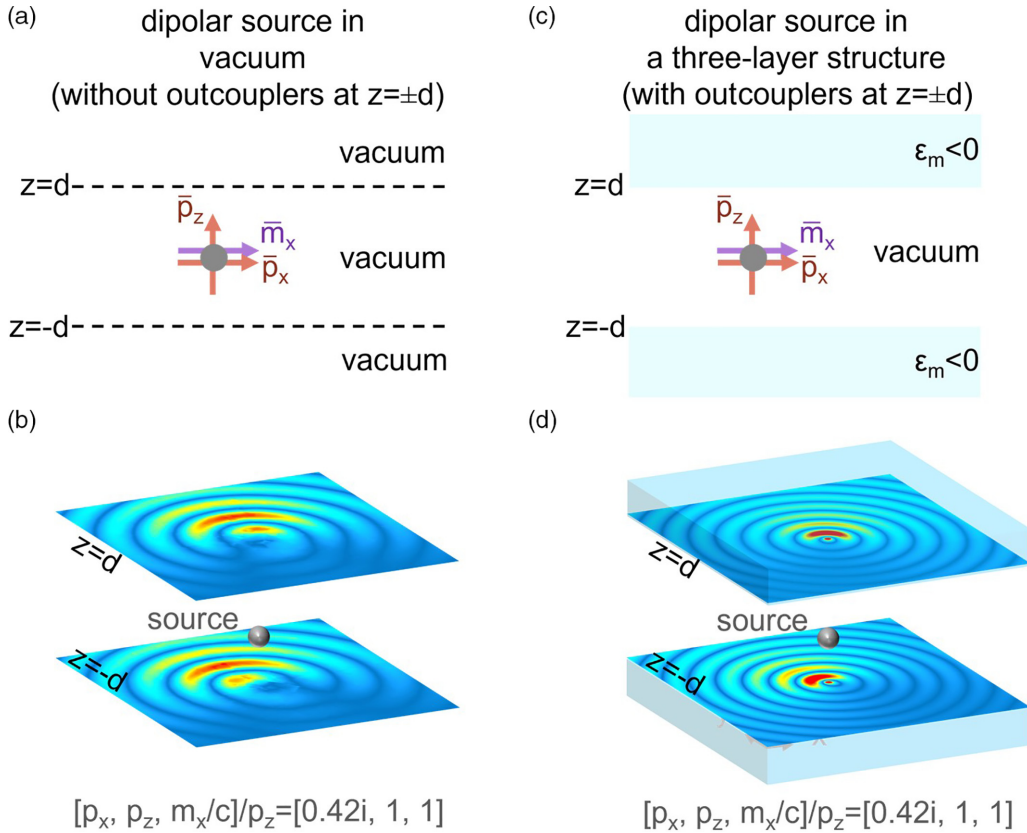
$[p_x, p_z, m_x/c]/p_z = [0.42i, 1, 1]$

FIG. 12. Complementary information for Fig. 4(a). The structural setup is the same as Fig. 4(a), except for the surrounding environment of the dipolar source. (a), (b) Near-field and far-field distribution of a dipolar source with $[p_x, p_z, m_x/c]/p_z = [0.42i, 1, 1]$ in free space. (c), (d) Field distribution of excited surface waves when this dipolar source is in a three-layer structure. To facilitate the comparison between the results in (a), (b) and Fig. 4(a), the results in (c), (d) are exactly adopted from Fig. 4(a).
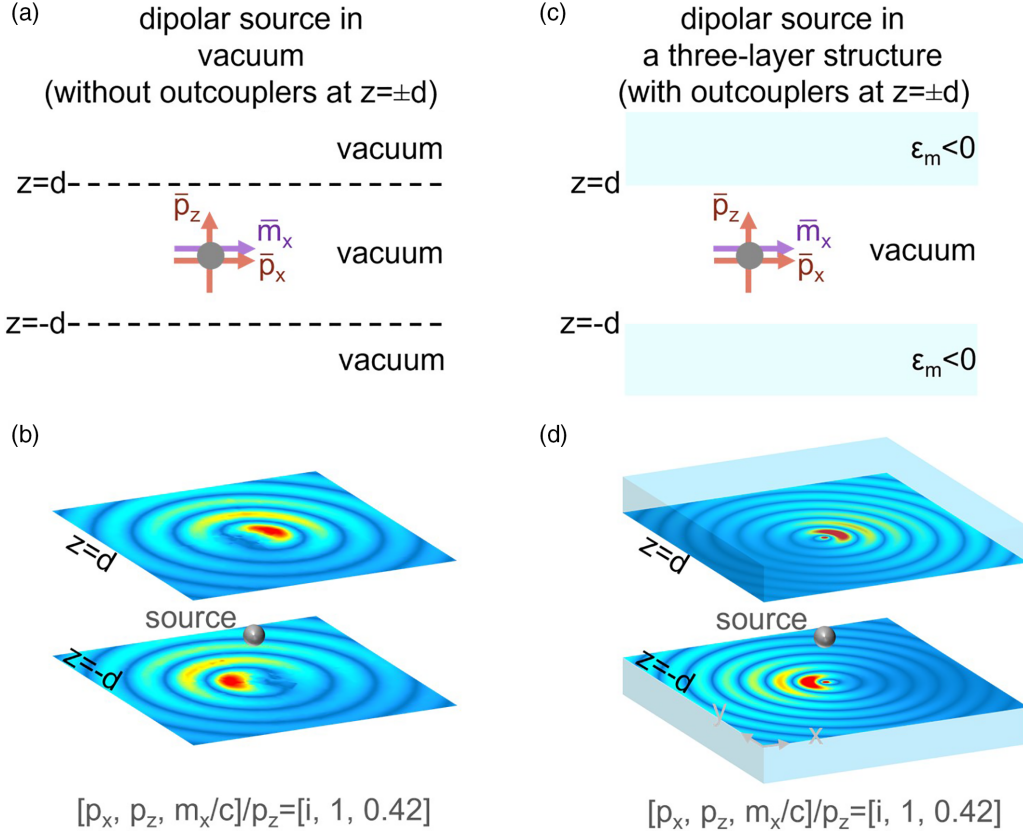
FIG. 13. Complementary information for Fig. 4(b). The structural setup is the same as Fig. 4(b), except for the surrounding environment of the dipolar source. (a), (b) Near-field and far-field distribution of a dipolar source with $[p_x, p_z, m_x/c]/p_z = [i, 1, 0.42]$ in free space. (c), (d) Field distribution of excited surface waves when this dipolar source is in a three-layer structure. To facilitate the comparison between the results in (a), (b) and Fig. 4(b), the results in (c), (d) are exactly adopted from Fig. 4(b).

Accordingly, we have $\phi_{\max}^{\text{lower}}$ which can be expressed as

$$\left(-\frac{ik_0}{k_{z,\text{sw}}} \frac{m_x/c}{p_x} \right) \phi_{\max}^{\text{lower}} = \arg\left(\frac{k_{\rho,\text{sw}}}{k_{z,\text{sw}}} \frac{p_z}{p_x} \right) + 2m_{\text{lower}}\pi, \quad \text{(F5)}$$

where m_{lower} is an integer to ensure $\phi_{\max}^{\text{lower}} \in [0°, 360°]$. Upon close inspection of Eqs. (F3) and (F5), mathematically, we

have

$$\left| \phi_{\max}^{\text{lower}} - \phi_{\max}^{\text{upper}} \right| = 2\arg\left(\frac{k_{\rho,\text{sw}}}{k_{z,\text{sw}}} \frac{p_z}{p_x} \right) - \pi + 2m_{\text{lower}}^{\text{upper}}\pi, \quad \text{(F6)}$$

where $m_{\text{lower}}^{\text{upper}}$ is an integer to ensure $\left| \phi_{\max}^{\text{lower}} - \phi_{\max}^{\text{upper}} \right| \in [0°, 360°]$.

Accordingly, the twist angle for Janus faces of dipolar sources in directional near-field coupling can be defined as

$$\phi_{\text{twist}} = \begin{cases} \text{mod}\left(\left| \phi_{\max}^{\text{lower}} - \phi_{\max}^{\text{upper}} \right|, 360° \right), & \text{if } \text{mod}\left(\left| \phi_{\max}^{\text{lower}} - \phi_{\max}^{\text{upper}} \right|, 360° \right) \in [0°, 180°] \\ 360° - \text{mod}\left(\left| \phi_{\max}^{\text{lower}} - \phi_{\max}^{\text{upper}} \right|, 360° \right), & \text{if } \text{mod}\left(\left| \phi_{\max}^{\text{lower}} - \phi_{\max}^{\text{upper}} \right|, 360° \right) \in [180°, 360°] \end{cases}. \quad \text{(F7)}$$

APPENDIX G: MORE DISCUSSION ON OTHER DIPOLAR SOURCES

Regarding the dipolar source with $[p_x, p_z, m_y/c] = [i, 1, b_m]$, the resultant near-field radiation patterns are plotted in Figs. 11(a)–11(h) with various values of b_m. According to Fig. 11, four distinct cases can be obtained. First, both the upper and lower near-field radiation patterns have no clear directionalities along the $\hat{x}$ direction; see Figs. 11(a) and 11(h) with $b_m = \pm 100$, for example. Second, either the upper or lower near-field radiation pattern has no clear

directionality along the $\hat{x}$ direction, such as those in Figs. 11(c) and 11(f) with $b_m = \pm 1$. Third, both the upper and lower near-field radiation patterns have clear directionalities along the $\hat{x}$ direction and have a twist angle $\phi_{\text{twist}} = 0°$, such as those in Figs. 11(b) and 11(g) with $b_m = \pm 10$. Fourth, both the upper and lower near-field radiation patterns have clear directionalities along the $\hat{x}$ direction and have a twist angle $\phi_{\text{twist}} = 180°$, such as those in Figs. 11(d) and 11(e) with $b_m = \pm 0.1$. In short, the dipolar source with $[p_x, p_z, m_y/c] = [i, 1, b_m]$ cannot realize the complete control of the twist angle.

APPENDIX H: MORE DISCUSSION ON FIG. 4

To facilitate the understanding of the results in Figs. 4(a) and 4(b), the near-field and far-field distributions of the corresponding dipolar source in free space are plotted in Figs. 12 and 13, respectively, which serve as the complementary information for Figs. 4(a) and 4(b). The near-field distribution of the dipolar source in free space in Figs. 12 and 13 might provide some qualitative guidance for understanding the results in Figs. 4(a) and 4(b).

[1] F. J. Rodríguez-Fortuño, G. Marino, P. Ginzburg, D. O'Connor, A. Martínez, G. A. Wurtz, and A. V. Zayats, Near-field interference for the unidirectional excitation of electromagnetic guided modes, Science **340**, 328 (2013).

[2] S.-Y. Lee, I.-M. Lee, J. Park, S. Oh, W. Lee, K.-Y. Kim, and B. Lee, Role of magnetic induction currents in nanoslit excitation of surface plasmon polaritons, Phys. Rev. Lett. **108**, 213907 (2012).

[3] A. H. Dorrah and F. Capasso, Tunable structured light with flat optics, Science **376**, eabi6860 (2022).

[4] J. Lin, J. P. B. Mueller, Q. Wang, G. Yuan, N. Antoniou, X.-C. Yuan, and F. Capasso, Polarization-controlled tunable directional coupling of surface plasmon polaritons, Science **340**, 331 (2013).

[5] X. Shi, X. Lin, I. Kaminer, F. Gao, Z. Yang, J. D. Joannopoulos, M. Soljačić, and B. Zhang, Superlight inverse Doppler effect, Nat. Phys. **14**, 1001 (2018).

[6] B. Kannan, A. Almanakly, Y. Sung, A. Di Paolo, D. A. Rower, J. Braumüller, A. Melville, B. M. Niedzielski, A. Karamlou, K. Serniak, A. Vepsäläinen, M. E. Schwartz, J. L. Yoder, R. Winik, J. I. J. Wang, T. P. Orlando, S. Gustavsson, J. A. Grover, and W. D. Oliver, On-demand directional microwave photon emission using waveguide quantum electrodynamics, Nat. Phys. **19**, 394 (2023).

[7] E. S. Redchenko, A. V. Poshakinskiy, R. Sett, M. Žemlička, A. N. Poddubny, and J. M. Fink, Tunable directional photon scattering from a pair of superconducting qubits, Nat. Commun. **14**, 2998 (2023).

[8] X. Lin and B. Zhang, Normal Doppler frequency shift in negative refractive-index systems, Laser Photon. Rev. **13**, 1900081 (2019).

[9] P. Lodah, S. Mahmoodian, S. Stobbe, A. Rauschenbeutel, P. Schneeweiss, J. Volz, H. Pichler, and P. Zoller, Chiral quantum optics, Nature (London) **541**, 473 (2017).

[10] A. Rauschenbeutel and P. Schneeweiss, Chiral quantum optics goes electric, Nat. Photon. **16**, 261 (2022).

[11] S. Zhang, J. Huang, Y. Yu, S. Wang, T. Yang, Z. Zhang, L. Tong, and J. Zhang, Quantum interference directed chiral Raman scattering in two-dimensional enantiomers, Nat. Commun. **13**, 1254 (2022).

[12] X. Zhang, Y. Liu, J. Han, Y. Kivshar, and Q. Song, Chiral emission from resonant metasurfaces, Science **377**, 1215 (2022).

[13] S. D. Namgung, R. M. Kim, Y.-C. Lim, J. W. Lee, N. H. Cho, H. Kim, J.-S. Huh, H. Rhee, S. Nah, M.-K. Song, J.-Y. Kwon, and K. T. Nam, Circularly polarized light-sensitive, hot electron transistor with chiral plasmonic nanoparticles, Nat. Commun. **13**, 5081 (2022).

[14] W. Bogaerts, D. Pérez, J. Capmany, D. A. B. Miller, J. Poon, D. Englund, F. Morichetti, and A. Melloni, Programmable photonic circuits, Nature (London) **586**, 207 (2020).

[15] Z. Zheng, H. Hu, Z. Zhang, B. Liu, M. Li, D.-H. Qu, H. Tian, W.-H. Zhu, and B. L. Feringa, Digital photoprogramming of liquid-crystal superstructures featuring intrinsic chiral photoswitches, Nat. Photon. **16**, 226 (2022).

[16] Z. Huang, Z. He, B. Ding, H. Tian, and X. Ma, Photoprogrammable circularly polarized phosphorescence switching of chiral helical polyacetylene thin films, Nat. Commun. **13**, 7841 (2022).

[17] Q. Tan, C. Qian, and H. Chen, Inverse-designed metamaterials for on-chip combinational optical logic circuit, Prog. Electromagn. Res. **176**, 55 (2023).

[18] Y. Long, J. Ren, Z. Guo, H. Jiang, Y. Wang, Y. Sun, and H. Chen, Designing all-electric subwavelength metasources for near-field photonic routings, Phys. Rev. Lett. **125**, 157401 (2020).

[19] M. Picardi, C. McPolin, J. Kingsley-Smith, X. Zhang, S. Xiao, F. Rodríguez-Fortuño, and A. Zayats, Integrated Janus dipole source for selective coupling to silicon waveguide networks, Appl. Phys. Rev. **9**, 021410 (2022).

[20] C. Wu, S. Kumar, Y. Kan, D. Komisar, Z. Wang, S. I. Bozhevolnyi, and F. Ding, Room-temperature on-chip orbital angular momentum single-photon sources, Sci. Adv. **8**, abk3075 (2022).

[21] L. Shen, X. Lin, M. Y. Shalaginov, T. Low, X. Zhang, B. Zhang, and H. Chen, Broadband enhancement of on-chip single-photon extraction via tilted hyperbolic metamaterials, Appl. Phys. Rev. **7**, 021403 (2020).

[22] J. Petersen, J. Volz, and A. Rauschenbeutel, Chiral nanophotonic waveguide interface based on spin-orbit interaction of light, Science **346**, 67 (2014).

[23] L. Huang, X. Chen, B. Bai, Q. Tan, G. Jin, T. Zentgraf, and S. Zhang, Helicity dependent directional surface plasmon polariton excitation using a metasurface with interfacial phase discontinuity, Light: Sci. Appl. **2**, e70 (2013).

[24] M. F. Picardi, M. Neugebauer, J. S. Eismann, G. Leuchs, P. Banzer, F. J. Rodríguez-Fortuño, and A. V. Zayats, Experimental demonstration of linear and spinning Janus dipoles for polarisation- and wavelength-selective near-field coupling, Light: Sci. Appl. **8**, 52 (2019).

[25] D. Yao, P. He, H. Zhang, J. Zhu, M. Hu, and T.-J. Cui, Miniaturized photonic and microwave integrated circuits based on surface plasmon polaritons, Prog. Electromagn. Res. **175**, 105 (2022).

[26] Y. Long, H. Ge, D. Zhang, X. Xu, J. Ren, M.-H. Lu, M. Bao, H. Chen, and Y.-F. Chen, Symmetry selective directionality in near-field acoustics, Natl. Sci. Rev. **7**, 1024 (2020).

[27] Y. Jiang, X. Lin, T. Low, B. Zhang, and H. Chen, Group-velocity-controlled and gate-tunable directional excitation of polaritons in graphene-boron nitride heterostructures, Laser Photon. Rev. **12**, 1800049 (2018).

[28] J. S. Eismann, L. H. Nicholls, D. J. Roth, M. A. Alonso, P. Banzer, F. J. Rodríguez-Fortuño, A. V. Zayats, F. Nori, and K. Y. Bliokh, Transverse spinning of unpolarized light, Nat. Photon. **15**, 156 (2021).

[29] A. Hassanfiroozi, Y. C. Cheng, S. H. Huang, Y. T. Lin, P. S. Huang, Y. Shi, and P. C. Wu, Toroidal-assisted generalized Huygens' sources for highly transmissive plasmonic metasurfaces, Laser Photon. Rev. **16**, 2100525 (2022).

[30] M. F. Picardi, A. V. Zayats, and F. J. Rodriguez-Fortuno, Janus and Huygens dipoles: Near-field directionality beyond spin-momentum locking, Phys. Rev. Lett. **120**, 117402 (2018).

[31] Y. Cheng, K. A. Oyesina, B. Xue, D. Lei, A. M. H. Wong, and S. Wang, Directional dipole dice enabled by anisotropic chirality, Proc. Natl. Acad. Sci. USA **120**, e2301620120 (2023).

[32] Y. Zhong, X. Lin, J. Jiang, Y. Yang, G.-G. Liu, H. Xue, T. Low, H. Chen, and B. Zhang, Toggling near-field directionality via polarization control of surface waves, Laser Photon. Rev. **15**, 2000388 (2021).

[33] Y. Jiang, X. Lin, and H. Chen, Directional polaritonic excitation of circular, Huygens and Janus dipoles in graphene-hexagonal boron nitride heterostructures, Prog. Electromagn. Res. **170**, 169 (2021).

[34] Y. Zhong, C. Wang, C. Bian, X. Chen, J. Chen, X. Zhu, H. Hu, T. Low, H. Chen, B. Zhang, and X. Lin, Dipole-matter interactions governed by the asymmetry of Maxwell equations, arXiv:2301.12718.

[35] M. F. Picardi, A. V. Zayats, and F. J. Rodríguez-Fortuño, Not every dipole is the same: The hidden patterns of dipolar near fields, Europhys. News **49**, 14 (2018).

[36] B.-J. Xiang and K.-M. Luk, A wideband low-profile folded transmitarray antenna based on magnetoelectric dipole elements, IEEE Trans. Antennas Propag. **71**, 8659 (2023).

[37] L. Ge and K.-M. Luk, A wideband magneto-electric dipole antenna, IEEE Trans. Antennas Propag. **60**, 4987 (2012).

[38] M.-C. Tang, Z. Wu, T. Shi, and R. W. Ziolkowski, Dual-band, linearly polarized, electrically small Huygens dipole antennas, IEEE Trans. Antennas Propag. **67**, 37 (2019).

[39] T. Han, B. Dong, Y. Zhang, Y. Wang, Z. Yan, H. Zhou, J. Feng, and Y. Liu, Research on the radiation properties of tapered slot magnetoelectric antenna, Prog. Electromagn. Res. **177**, 75 (2023).

[40] R. Alaee, R. Filter, D. Lehr, F. Lederer, and C. Rockstuhl, A generalized Kerker condition for highly directive nanoantennas, Opt. Lett. **40**, 2645 (2015).

[41] T. Coenen, F. Bernal Arango, A. Femius Koenderink, and A. Polman, Directional emission from a single plasmonic scatterer, Nat. Commun. **5**, 3250 (2014).

[42] I. M. Hancu, A. G. Curto, M. Castro-López, M. Kuttge, and N. F. vanHulst, Multipolar interference for directed light emission, Nano Lett. **14**, 166 (2014).

[43] A. B. Evlyukhin, S. M. Novikov, U. Zywietz, R. L. Eriksen, C. Reinhardt, S. I. Bozhevolnyi, and B. N. Chichkov, Demonstration of magnetic dipole resonances of dielectric nanospheres in the visible region, Nano Lett. **12**, 3749 (2012).

[44] A. I. Kuznetsov, A. E. Miroshnichenko, M. L. Brongersma, Y. S. Kivshar, and B. Luk'yanchuk, Optically resonant dielectric nanostructures, Science **354**, aag2472 (2016).

[45] D. Permyakov, I. Sinev, D. Markovich, P. Ginzburg, A. Samusev, P. Belov, V. Valuckas, A. I. Kuznetsov, B. S. Luk'yanchuk, A. E. Miroshnichenko, D. N. Neshev, and Y. S. Kivshar, Probing magnetic and electric optical responses of silicon nanoparticles, Appl. Phys. Lett. **106**, 171110 (2015).

[46] P. Woźniak, P. Banzer, and G. Leuchs, Selective switching of individual multipole resonances in single dielectric nanoparticles, Laser Photon. Rev. **9**, 231 (2015).

[47] U. Zywietz, A. B. Evlyukhin, C. Reinhardt, and B. N. Chichkov, Laser printing of silicon nanoparticles with resonant optical electric and magnetic responses, Nat. Commun. **5**, 3402 (2014).

[48] R. R. Chance, A. Prock, and R. Silbey, Molecular fluorescence and energy transfer near interfaces, Adv. Chem. Phys. **37**, 1 (1978).

[49] V. V. Klimov, D. V. Guzatov, and M. Ducloy, Engineering of radiation of optically active molecules with chiral nano-meta-particles, Europhys. Lett. **97**, 47004 (2012).

[50] D. V. Guzatov and V. V. Klimov, Spontaneous emission of an optically active molecule near a chiral nanoellipsoid, Phys. Rev. A **98**, 013823 (2018).

[51] V. V. Klimov, I. V. Zabkov, A. A. Pavlov, and D. V. Guzatov, Eigen oscillations of a chiral sphere and their influence on radiation of chiral molecules, Opt. Express. **22**, 18564 (2014).

[52] D. V. Guzatov, V. V. Klimov, and N. S. Poprykailo, Spontaneous radiation of a chiral molecule located near a half-space of a bi-isotropic material, J. Exp. Theor. Phys. **116**, 531 (2013).

[53] D. V. Guzatov, V. V. Klimov, H.-C. Chan, and G.-Y. Guo, Tuning spontaneous radiation of chiral molecules by asymmetric chiral nanoparticles, Opt. Express **25**, 6036 (2017).

[54] M. F. Picardi, A. V. Zayats, and F. J. Rodríguez-Fortuño, Amplitude and phase control of guided modes excitation from a single dipole source: Engineering far- and near-field directionality, Laser Photon. Rev. **13**, 1900250 (2019).

[55] M. F. Picardi, A. Manjavacas, A. V. Zayats, and F. J. Rodríguez-Fortuño, Unidirectional evanescent-wave coupling from circularly polarized electric and magnetic dipoles: An angular spectrum approach, Phys. Rev. B **95**, 245416 (2017).

[56] Y. Cao, V. Fatemi, S. Fang, K. Watanabe, T. Taniguchi, E. Kaxiras, and P. Jarillo-Herrero, Unconventional superconductivity in magic-angle graphene superlattices, Nature (London) **556**, 43 (2018).

[57] E. Y. Andrei and A. H. MacDonald, Graphene bilayers with a twist, Nat. Mater. **19**, 1265 (2020).

[58] S. Turkel, J. Swann, Z. Zhu, M. Christos, K. Watanabe, T. Taniguchi, S. Sachdev, M. S. Scheurer, E. Kaxiras, C. R. Dean, and A. N. Pasupathy, Orderly disorder in magic-angle twisted trilayer graphene, Science **376**, 193 (2022).

[59] Z. Hao, A. M. Zimmerman, P. Ledwith, E. Khalaf, D. H. Najafabadi, K. Watanabe, T. Taniguchi, A. Vishwanath, and P. Kim, Electric field-tunable superconductivity in alternating-twist magic-angle trilayer graphene, Science **371**, 1133 (2021).

[60] A. Jorio, Twistronics and the small-angle magic, Nat. Mater. **21**, 844 (2022).

[61] X. Lin, S. Lin, Y. Xu, and H. Chen, Electronic structures of multilayer two-dimensional silicon carbide with oriented mis-alignment, J. Mater. Chem. C **3**, 9057 (2015).

[62] D. M. Kennes, M. Claassen, L. Xian, A. Georges, A. J. Millis, J. Hone, C. R. Dean, D. N. Basov, A. N. Pasupathy, and A. Rubio, Moiré heterostructures as a condensed-matter quantum simulator, Nat. Phys. **17**, 155 (2021).

[63] L. Du, M. R. Molas, Z. Huang, G. Zhang, F. Wang, and Z. Sun, Moiré photonics and optoelectronics, Science **379**, eadg0014 (2023).

[64] Z. Meng, L. Wang, W. Han, F. Liu, K. Wen, C. Gao, P. Wang, C. Chin, and J. Zhang, Atomic Bose-Einstein condensate in twisted-bilayer optical lattices, Nature (London) **615**, 231 (2023).

[65] Y. Meng, J. Feng, S. Han, Z. Xu, W. Mao, T. Zhang, J. S. Kim, I. Roh, Y. Zhao, D.-H. Kim, Y. Yang, J.-W. Lee, L. Yang, C.-W. Qiu, and S.-H. Bae, Photonic van der Waals integration from 2D materials to 3D nanomembranes, Nat. Rev. Mater. **8**, 498 (2023).

[66] Q. Zhang, G. Hu, W. Ma, P. Li, A. Krasnok, R. Hillenbrand, A. Alù, and C.-W. Qiu, Interface nano-optics with van der Waals polaritons, Nature (London) **597**, 187 (2021).

[67] G. Hu, Q. Ou, G. Si, Y. Wu, J. Wu, Z. Dai, A. Krasnok, Y. Mazor, Q. Zhang, Q. Bao, C.-W. Qiu, and A. Alù, Topological polaritons and photonic magic angles in twisted α-MoO$_3$ bilayers, Nature (London) **582**, 209 (2020).

[68] M. Chen, X. Lin, T. H. Dinh, Z. Zheng, J. Shen, Q. Ma, H. Chen, P. Jarillo-Herrero, and S. Dai, Configurable phonon polaritons in twisted α-MoO$_3$, Nat. Mater. **19**, 1307 (2020).

[69] B. Lou, N. Zhao, M. Minkov, C. Guo, M. Orenstein, and S. Fan, Theory for twisted bilayer photonic crystal slabs, Phys. Rev. Lett. **126**, 136101 (2021).

[70] J. Chen, X. Lin, M. Chen, T. Low, H. Chen, and S. Dai, A perspective of twisted photonic structures, Appl. Phys. Lett. **119**, 240501 (2021).

[71] X. Lin, Z. Liu, T. Stauber, G. Gómez-Santos, F. Gao, H. Chen, B. Zhang, and T. Low, Chiral plasmons with twisted atomic bilayers, Phys. Rev. Lett. **125**, 077401 (2020).

[72] Q. Fu, P. Wang, C. Huang, Y. V. Kartashov, L. Torner, V. V. Konotop, and F. Ye, Optical soliton formation controlled by angle twisting in photonic moiré lattices, Nat. Photon. **14**, 663 (2020).

[73] M. Kerker, D.-S. Wang, and C. L. Giles, Electromagnetic scattering by magnetic spheres, J. Opt. Soc. Am. **73**, 765 (1983).

[74] R. Paniagua-Domínguez, Y. F. Yu, A. E. Miroshnichenko, L. A. Krivitsky, Y. H. Fu, V. Valuckas, L. Gonzaga, Y. T. Toh, A. Y. S. Kay, B. Luk'yanchuk, and A. Kuznetsov, Generalized Brewster effect in dielectric metasurfaces, Nat. Commun. **7**, 10362 (2016).

[75] J. M. Geffrin, B. García-Cámara, R. Gómez-Medina, P. Albella, L. S. Froufe-Pérez, C. Eyraud, A. Litman, R. Vaillon, F. González, M. Nieto-Vesperinas, J. J. Sáenz, and F. Moreno, Magnetic and electric coherence in forward- and back-scattered electromagnetic waves by a single dielectric subwavelength sphere, Nat. Commun. **3**, 1171 (2012).

[76] Y. H. Fu, A. I. Kuznetsov, A. E. Miroshnichenko, Y. F. Yu, and B. Luk'yanchuk, Directional visible light scattering by silicon nanoparticles, Nat. Commun. **4**, 1527 (2013).

[77] V. V. Klimov and M. Ducloy, Quadrupole transitions near interface: General theory and application to atom inside a planar cavity, Phys. Rev. A **72**, 043809 (2005).